JCB Journal of Cell Biology

ARTICLE

An interkinetic envelope surrounds chromosomes between meiosis I and II in *C. elegans* oocytes

Layla El Mossadeq[1], Laura Bellutti[1], Rémi Le Borgne[1], Julie C. Canman[2], Lionel Pintard[1], Jean-Marc Verbavatz[1], Peter Askjaer[3], and Julien Dumont[1]

At the end of cell division, the nuclear envelope reassembles around the decondensing chromosomes. Female meiosis culminates in two consecutive cell divisions of the oocyte, meiosis I and II, which are separated by a brief transition phase known as interkinesis. Due to the absence of chromosome decondensation and the suppression of genome replication during interkinesis, it has been widely assumed that the nuclear envelope does not reassemble between meiosis I and II. By analyzing interkinesis in *C. elegans* oocytes, we instead show that an atypical structure made of two lipid bilayers, which we termed the interkinetic envelope, surrounds the surface of the segregating chromosomes. The interkinetic envelope shares common features with the nuclear envelope but also exhibits specific characteristics that distinguish it, including its lack of continuity with the endoplasmic reticulum, unique protein composition, assembly mechanism, and function in chromosome segregation. These distinct attributes collectively define the interkinetic envelope as a unique and specialized structure that has been previously overlooked.

Introduction

The nuclear envelope delineates the nucleus in all eukaryotic cells. It comprises two lipid bilayers that form the inner nuclear membrane (INM) in contact with chromatin and the outer nuclear membrane (ONM) facing the cytoplasm (Hetzer, 2010). The INM, lined by the nuclear lamina, faces the nucleoplasmic compartment and features a unique set of proteins, including the LAP2, Emerin, and MAN1 (LEM)-domain integral membrane proteins (Ungricht and Kutay, 2015). The ONM connects to the endoplasmic reticulum (ER) and shares both compomisition and function with the ER (Deolal et al., 2024). The INM is fused with the ONM at designated sites where multisubunit macromolecular complexes, known as nuclear pore complexes (NPCs), assemble and facilitate nucleocytoplasmic transport across the nuclear envelope (De Magistris and Antonin, 2018; Ungricht and Kutay, 2017). The linker of nucleoskeleton and cytoskeleton (LINC) complex, a highly conserved 6:6 heterohexameric bridge spanning the nuclear envelope, serves to physically connect chromatin and the nuclear lamina to the cytoskeleton (McGillivary et al., 2023).

In organisms undergoing semiopen or open mitosis, the transition from interphase to mitosis (M-phase) is marked by nuclear envelope breakdown (NEBD) and chromosome condensation (Boettcher and Barral, 2013). Following chromosome segregation, the nuclear envelope must reassemble around the decondensing chromatids to separate the genome from the cytoplasmic environment. Thus, cycles of NEBD and chromosome condensation, followed by nuclear envelope reassembly around decondensing chromatids, accompany successive cell divisions in most tissues and cell types. A notable deviation from this stereotypical sequence of events occurs during oogenesis, which culminates in two consecutive cell divisions of the oocyte known as meiosis I and II (Dumont and Desai, 2012; Mullen et al., 2019; Ohkura, 2015; Severson et al., 2016). During meiosis I, recombined homologous chromosome pairs are segregated into two chromosome sets. One set is directed for elimination into the first polar body (hereafter referred to as the PB chromosomal set), while the second set (the MII chromosomal set) almost immediately proceeds to meiosis II, following a very brief transition phase termed interkinesis. A remarkable feature of interkinesis is the apparent lack of chromosome decondensation preceding entry into meiosis II and the segregation of sister chromatids (Nakajo et al., 2000). This is coupled with the suppression of genome replication, which normally occurs after exiting from the M-phase and which is essential in this specific context for generating haploid oocytes (Furuno et al., 1994). Hence, although interkinesis occurs between two M-phases, it is

[1]Université Paris Cité, CNRS, Institut Jacques Monod, Paris, France; [2]Department of Pathology and Cell Biology, Columbia University, New York, NY, USA; [3]Andalusian Center for Developmental Biology, CSIC/JA/Universidad Pablo de Olavide, Seville, Spain.

Correspondence to Julien Dumont: julien.dumont@ijm.fr.

not classified as a typical interphase. In this context, the status of the nuclear envelope during interkinesis remains notably ambiguous (Gerhart et al., 1984; Lénárt and Ellenberg, 2003; Nakajo et al., 2000; Nebreda and Ferby, 2000). As interkinesis occurs between two M-phases, one would anticipate nuclear envelope reassembly at this stage. Yet, the apparent suppression of most interphase events and the scarcity of reports on the presence of a canonical nuclear envelope surrounding oocyte chromosomes during interkinesis in any species has led to controversy over its actual existence (Penfield et al., 2020).

In this study, we probed nuclear envelope reassembly in oocytes of the nematode *Caenorhabditis elegans* during interkinesis. We found that a novel organelle superficially reminiscent of the nuclear envelope, which we termed the interkinetic envelope, progressively assembles at the surface of the segregating chromosomes during interkinesis.

Results

An interkinetic envelope forms on the surface of both chromosomal sets between meiosis I and II in oocytes

To determine if a nuclear envelope reassembles during the short interkinetic transition phase between meiosis I and II in *C. elegans* oocytes, we analyzed the three-dimensional organization of membranes around chromosomes during anaphase I/interkinesis by correlative light and serial block-face scanning electron microscopy (SBF-SEM) (Lachat et al., 2022). Fertilized oocytes expressing green fluorescent protein (GFP)–tagged tubulin and mCherry-tagged H2B were imaged ex utero using a spinning disk microscope until they reached mid-anaphase I or mid-/late interkinesis (Fig. 1 A). They were then fixed chemically and processed for SBF-SEM. 30-nm-thick sections were automatically cut and imaged throughout the two sets of segregating chromosomes, and a slab of each stage oocyte including both sets of chromosomes was reconstructed (Fig. 1 B and Video 1).

In the earlier mid-anaphase I oocyte, vesicular membranous structures were observed on the surface of both chromosome sets. These structures formed two discontinuous double membrane layers that covered the outer surfaces. These double membrane layers were seen surrounding both the extruded chromosomal set (facing the plasma membrane of the future PB) and the meiosis II chromosomal set (facing the oocyte cytoplasm [MII]). They were excluded from the chromosomal surfaces facing the central spindle region of both chromosomal sets. As meiosis I progressed into mid-interkinesis, the double membrane layer enveloping the MII chromosomal set displayed increased continuity, with both the mean and total lengths of membrane contours continuously expanding until late interkinesis (Fig. 1, C and D). After the extrusion of the first polar body between mid- and late interkinesis, the mean length of membrane contours stagnated. The initial increase in mean contour length suggested that double membrane fragments likely expand or fuse to generate longer fragments. In contrast, after this initial phase, the stagnation in mean contour length, coupled with the ever-increasing total length of contours, suggested that additional membrane fragments are likely recruited to the surface of chromosomal sets between mid- and late interkinesis. The overall length of membrane contours on the PB chromosomal set remained comparatively stable during anaphase I/interkinesis but completely disappeared as late interkinesis ensued (Fig. 1 C). Importantly, upon reexamination of the tomographic electron microscopy data that we had previously conducted to analyze microtubule organization during anaphase/telophase I in high-pressure frozen *C. elegans* oocytes (Laband et al., 2017), we identified identical vesicular and membranous structures on the surface of chromosomes (Fig. S1 A). The overall characteristics and dynamics of membranes were thus not significantly disrupted by the chemical fixation procedure employed in our SBF-SEM observations. These results suggest that an asymmetric double membrane structure, reminiscent of the nuclear envelope, appears progressively during interkinesis at the chromosomal surface and disappears shortly after PB extrusion.

We next probed the nature and precise kinetics of assembly of this membranous structure by time-lapse imaging of fertilized oocytes from a *C. elegans* transgenic strain co-expressing the nuclear envelope marker and INM LEM-domain protein LEM-2$^{LEMD2/3}$ fused to GFP and histone H2B fused to mCherry (Fig. 1 E and Video 2) (Brachner et al., 2005; Lee et al., 2000; Lin et al., 2000). Surprisingly, LEM-2$^{LEMD2/3}$ localized asymmetrically to the different chromosomal sets. Unlike the double membrane structures observed in our EM analysis, LEM-2$^{LEMD2/3}$ was only faintly detectable on the surface of the PB chromosomal set during both meiotic divisions. In stark contrast, following the onset of anaphase I, LEM-2$^{LEMD2/3}$ gradually accumulated on the exterior surface of the MII chromosomal set, which correlated with the location of the membranous structure identified by SBF-SEM (Penfield et al., 2020). At mid-interkinesis, LEM-2$^{LEMD2/3}$ enveloped the surface of the MII chromosomal set and reached its peak intensity. In late interkinesis, it gradually diminished from the MII chromosomal surface, only to reappear during the onset of anaphase II. Consistent with an earlier observation, we noted a robust accumulation of LEM-2$^{LEMD2/3}$ at the end of anaphase II on the inner (central spindle facing) surface of the decondensing maternal pronucleus (Penfield et al., 2020). This accumulating LEM-2$^{LEMD2/3}$ appeared to form a distinct “plaque”-like structure, which is the recruitment site of ESCRT-III complex proteins, such as CHMP-7^{CHMP7} and VPS-32^{CHMP4} (Fig. 1 E, cyan arrows) (Gatta and Carlton, 2019; Gu et al., 2017; Penfield et al., 2020). These ESCRT-III proteins are involved in the remodeling and sealing of the nuclear envelope proximal to the central spindle (Barger et al., 2023; Penfield et al., 2020). We did not observe any LEM-2$^{LEMD2/3}$ plaque-like structure nor the accumulation of CHMP-7^{CHMP7} or VPS-32^{CHMP4} during interkinesis (Fig. S1 B). This observation aligned with the absence of double membrane sealing in our late interkinesis SBF-SEM reconstruction, indicating that, unlike a typical nuclear envelope, double membranes never fully enclose the MII chromosomal set during interkinesis. Therefore, we chose the term “”interkinetic envelope” to describe this unique, asymmetric, and non-canonical membranous structure.

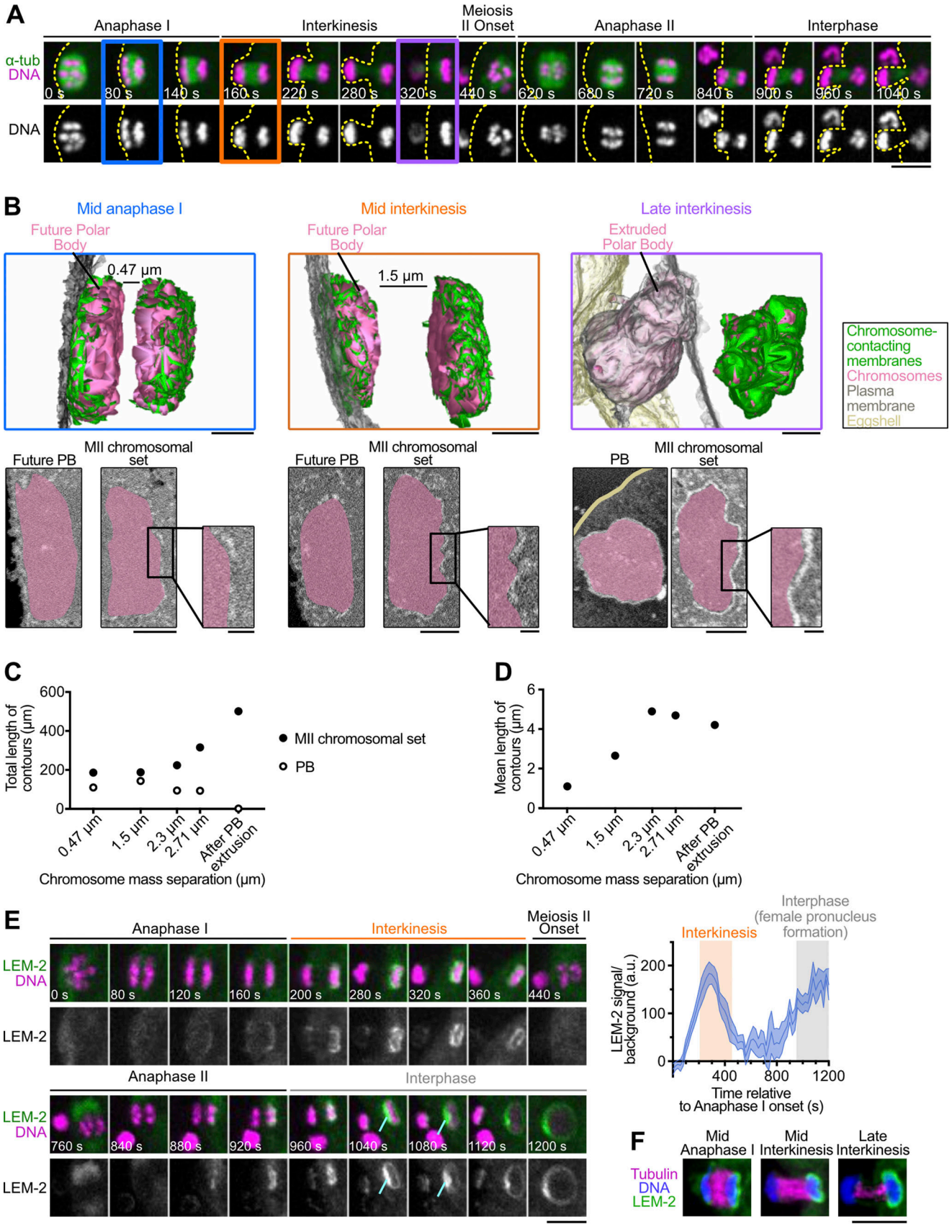

Figure 1. **The interkinetic envelope forms between meiosis I and II in the *C. elegans* oocyte. (A)** Representative time-lapse images of GFP::TBA-2$^{\alpha\text{-tubulin}}$ (green) and mCherry::HIS-11^{H2B} (magenta)–expressing oocytes during meiosis I and II (n = 7). Timings indicated at the bottom left corners of images are from

anaphase I onset. The specific meiotic stages used for electron microscopy are highlighted in blue (mid-anaphase), orange (mid interkinesis), and purple (late interkinesis). Scale bar, 5 µm. **(B)** Three-dimensional reconstructions centered on chromosomes of a mid-anaphase I (left, *n* = 1), a mid-interkinesis (center, *n* = 1), and a late-interkinesis (right, *n* = 1) oocytes acquired by SBF-SEM. Chromosomes in magenta, membranes in contact with chromosomes in green, plasma membrane in gray, and eggshell in gold. Each reconstruction is accompanied (bottom) by a two-dimensional single section showing each chromosome set in magenta and a magnification of a region of interest (ROI) of the MII chromosomal set. Scale bar, 1 µm for the full view, 0.25 µm for the magnification. **(C and D)** Quantifications of the total (C) and mean (D) length of membrane contours from five reconstructed oocytes represented according to the distance between the segregating chromosomal sets (chromosome mass separation) for the PB chromosomal set (empty dots) and for the MII chromosomal set (solid dots). **(E)** Left: Representative time-lapse images of GFP::LEM-2$^{LEMD2/3}$ and mCherry::H2B–expressing oocytes (*n* = 9) during meiosis I (top) and meiosis II (bottom). Timing relative to anaphase I onset is indicated at the bottom left corner of each image. The cyan arrows indicate the GFP::LEM-2$^{LEMD2/3}$ plaque. Scale bar, 5 µm. Right: Quantification of the normalized GFP::LEM-2$^{LEMD2/3}$ integrated intensity over time from anaphase I onset to interphase for the MII chromosomal set. Error bars correspond to the standard error of the mean. The orange and gray boxes indicate interkinesis and interphase, respectively. The same control oocyte is displayed in Fig. S2 E and Fig. S3 D. **(F)** Representative images centered on chromosomes of fixed oocytes showing the immunolocalization of LEM-2$^{LEMD2/3}$, DNA, and Tubulin in mid anaphase I, mid and late interkinesis. Scale bar, 5 µm.

Microtubules and proximity to the plasma membrane negatively regulate interkinetic envelope assembly

Next, we investigated the origin of the asymmetric assembly of the interkinetic envelope, which initiated on the external surface of chromosomes and was more pronounced on the MII compared with the PB chromosomal set. We previously demonstrated that in *C. elegans* oocytes, after anaphase onset, meiotic spindle pole microtubules disassemble before central spindle microtubules (Laband et al., 2017). This temporal uncoupling mirrors the observed asymmetry in interkinetic envelope assembly, which begins on the external (spindle pole facing) surface of chromosomes before progressing toward the internal (central spindle facing) surface (Fig. 1 F). This observation suggested a potential functional link between microtubule disassembly and interkinetic envelope assembly, similar to nuclear envelope reformation during mitotic exit (Dey and Baum, 2021). To directly test this hypothesis, we treated oocytes with a low dose of colchicine immediately after anaphase onset to promote microtubule disassembly while allowing chromosome segregation to continue. We then monitored the recruitment of GFP-tagged LEM-2$^{LEMD2/3}$ as a marker for interkinetic envelope assembly (Fig. S1 C). In colchicine-treated oocytes, LEM-2$^{LEMD2/3}$ was recruited more rapidly to the chromosome surface and formed a more continuous layer around the MII chromosomal set compared with controls. These results indicate that spindle microtubule disassembly triggers interkinetic envelope formation and prevents premature assembly on the internal surface of chromosomes.

The visible asymmetry between the MII and PB interkinetic envelopes mirrored the uneven positioning of the two chromosomal sets during anaphase and interkinesis. Specifically, the PB chromosomes were oriented toward the plasma membrane, while the MII chromosomes faced the oocyte cytoplasm (Fig. 1, B–E). This led us to hypothesize that the plasma membrane might act as a barrier, inhibiting or delaying interkinetic envelope assembly around the PB chromosomal set. To test this, we depleted the dynein adaptor protein LIN-5^{NuMA} via RNAi (Fig. S1 D). LIN-5^{NuMA} is crucial for recruiting dynein to meiotic spindle poles, which in turn is essential for microtubule focusing at the spindle poles and proper spindle rotation perpendicular to the plasma membrane before anaphase (van der Voet et al., 2009). In LIN-5^{NuMA}-depleted oocytes, the spindle remained parallel to the oocyte cortex and chromosome segregation occurred parallel to the plasma membrane. Strikingly, this was accompanied by a symmetrization of GFP-tagged LEM-2$^{LEMD2/3}$ levels between the two chromosomal sets compared to control oocytes, suggesting that proximity to the plasma membrane might hinder or delay LEM-2$^{LEMD2/3}$ recruitment and interkinetic envelope assembly on the PB chromosomal set. Taken together, our results suggest that both the anaphase I central spindle microtubules and the proximity of the plasma membrane negatively regulate LEM-2$^{LEMD2/3}$ recruitment and likely also the formation of the interkinetic envelope.

The interkinetic envelope contains INM but lacks ONM proteins

To determine the protein composition of the interkinetic envelope, we analyzed the localization of GFP-tagged INM and ONM proteins including the unique *C. elegans* B-type lamin protein LMN-1$^{Lamin\ B1}$, which lines the inner side of the INM (Liu et al., 2000), the second LEM-domain INM protein EMR-1^{Emerin} (Gruenbaum et al., 2002; Manilal et al., 1996; Nagano et al., 1996), the chromatin-binding protein BAF-1^{BAF} (Barrier of Autointegration Factor) responsible for LEM-domain protein recruitment to the INM (Gorjánácz et al., 2007; Shumaker et al., 2001), the two LINC complex components, SUN-1^{SUN1} at the INM and the KASH domain protein ZYG-12 at the ONM (Malone et al., 2003; Ungricht and Kutay, 2017), the ER signal peptidase and ONM marker SPCS-1^{SP12} (Poteryaev et al., 2005; Rolls et al., 2002), and the stress-associated endoplasmic reticulum protein 1 (SERP-1.1, also known as ribosome-associated membrane protein 4, RAMP4) (Lee et al., 2016) (Fig. 2, A and B; and Video 3). In addition to the single lamin LMN-1$^{Lamin\ B1}$, all INM proteins tested, including LEM-2$^{LEMD2/3}$, EMR-1^{Emerin}, BAF-1^{BAF}, and SUN-1^{SUN1} were located at the surface of the MII chromosomal set during interkinesis colocalizing with the interkinetic envelope, with BAF-1^{BAF} also localized all over the chromosome mass. Instead, ONM proteins ZYG-12, SPCS-1^{SP12}, and SERP-1.1^{RAMP4} were absent (Fig. 2, A–C). In the nuclear envelope, the ONM is continuous and functionally interrelated with the ER, with which it shares numerous proteins and markers (Whaley et al., 1960). The lack of ONM markers in the interkinetic envelope suggests that, unlike canonical nuclear envelopes, the interkinetic envelope is not contiguous with the ER. We confirmed this hypothesis by analyzing the ultrastructure of the ER, close to the interkinetic envelope, using SBF-SEM (Fig. 2 D and Video 4). Although ER membrane sheets were present near the MII chromosomal set throughout anaphase and interkinesis,

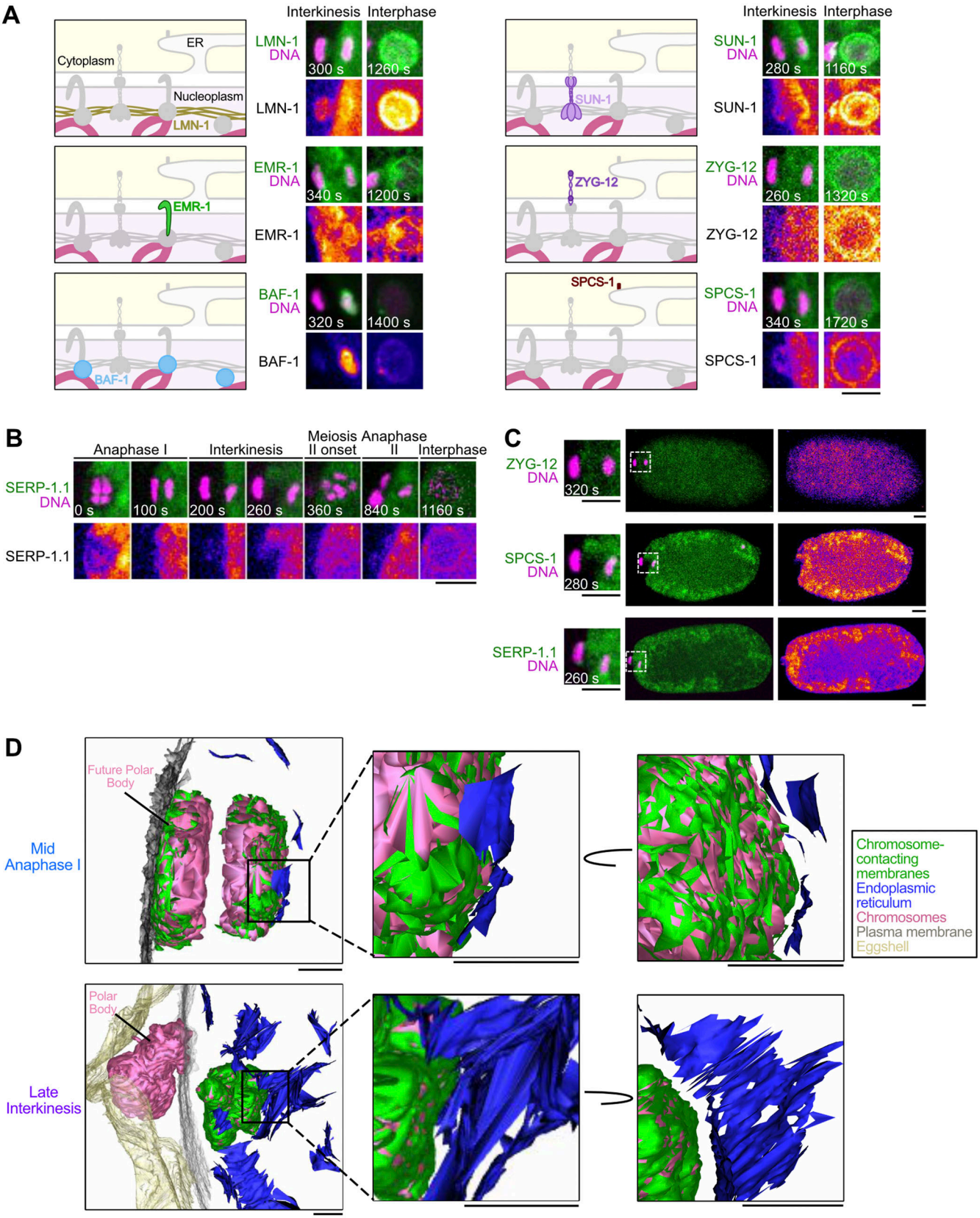

Figure 2. **The interkinetic envelope contains INM but lacks ONM proteins. (A)** Left: Schematics of INM and ONM protein theoretical localization at the nuclear envelope. Right: Representative images of an ROI centered around chromosomes from oocytes expressing mCherry::H2B and either GFP::EMR-1^{Emerin} (n = 6), GFP::BAF-1^{BAF} (n = 20), GFP::LMN-1^{LaminB1} (n = 7), SUN-1^{SUN1}::GFP (n = 17), GFP::ZYG-12 (n = 14), or GFP::SPCS-1^{SP12} (n = 18) during interkinesis and interphase. Timings indicated at the bottom left corner of images are from anaphase I onset. Scale bar, 5 µm. **(B)** Representative time-lapse images centered on

chromosomes of oocytes expressing mCherry::H2B (magenta) and GFP::SERP-1.1^{RAMP4} (green) (n = 6) during meiosis I and II. Timings indicated at the bottom left corners of images are from anaphase I onset. Scale bar, 5 µm. **(C)** Representative images of oocytes expressing mCherry::H2B (magenta) and either GFP::ZYG-12, GFP::SPCS-1^{SP12} or GFP::SERP-1.1^{RAMP4} (green) during interkinesis, with a magnification of the ROI (white dashed box) displayed on the left. **(D)** Left: Three-dimensional reconstructions centered on chromosomes of a mid-anaphase I (top) and a late interkinesis (bottom) oocyte acquired by SBF-SEM. Chromosomes in magenta, membranes in contact with chromosomes in green, plasma membrane in gray, eggshell in gold, and endoplasmic reticulum in blue. Right: Magnifications of an ROI viewed from two different angles to show the lack of continuity between the interkinetic envelope and the ER. Scale bars, 1 µm for the full view and 0.5 µm for the ROI.

they were visibly distinct and physically separated from the interkinetic envelope. Thus, the interkinetic envelope on the MII chromosomal set contains INM proteins but lacks ONM proteins, likely due to its physical disconnection from the ER.

BAF-1^{BAF} and VRK-1^{VRK1} control the structural integrity of the interkinetic envelope

Upon mitotic exit in both *C. elegans* and human cells, BAF plays a crucial role in nuclear envelope reformation (Asencio et al., 2012; Gorjánácz et al., 2007; Liu et al., 2003; Samwer et al., 2017; Schellhaus et al., 2016). To explore the potential involvement of the equivalent *C. elegans* protein in interkinetic envelope formation, we performed SBF-SEM following the full depletion of BAF-1^{BAF} in oocytes. Due to the inherent challenge of achieving full depletion through RNAi alone of a small 90-amino-acid protein such as BAF-1^{BAF}, we employed a dual approach, combining RNAi with auxin treatment in a transgenic strain engineered to express endogenous BAF-1^{BAF} fused to an AID (auxin-Inducible Degron) tag (Zhang et al., 2015) (Fig. S2, A and B). Complete depletion of BAF-1^{BAF}, achieved only through the combination of RNAi and auxin treatments, did not inhibit the formation of the interkinetic envelope (Fig. 3 A, Fig. S2, A–C, and Video 5). However, while control oocytes displayed a nearly continuous envelope covering the outer surface of the MII chromosomal set, BAF-1^{BAF}–depleted oocytes assembled a highly fenestrated envelope with a strong reduction in overall membrane density (total membrane length in contact with chromosomes in control oocytes was 325.24 µm versus 183.82 µm in the absence of BAF-1^{BAF}). Unlike in controls, in BAF-1^{BAF}–depleted oocytes, small membrane fragments covered the surface of both chromosomal sets and were found inside the chromatin masses of the segregating chromosomes (Fig. 3 A white arrows). Thus, BAF-1^{BAF} depletion leads to a drastic reduction in the recruitment of membranes necessary for interkinetic envelope assembly, coupled with strong defects in membrane fusion and distribution over both segregating chromosomal sets.

During nuclear envelope reformation, BAF mediates the physical interaction between chromatin and LEM-domain proteins, which is essential for nuclear envelope integrity (Gorjánácz et al., 2007; Liu et al., 2003). To determine if the phenotype we observed upon BAF-1^{BAF} depletion could be attributed to defects in LEM-domain protein recruitment, we employed RNAi to knock down BAF-1^{BAF} and monitored the presence of GFP-tagged INM proteins LEM-2$^{LEMD2/3}$ and EMR-1^{Emerin} (Fig. 3 B; Fig. S2, D and E; and Video 6). Depletion of BAF-1^{BAF} resulted in a significant reduction of both INM proteins from the interkinetic envelope. Together, these results suggest that BAF-1^{BAF} plays an important role in controlling the integrity and continuity of the interkinetic envelope, potentially by recruiting LEM-domain proteins on the chromatin surface. The structural integrity defects observed in the interkinetic envelope following BAF-1^{BAF} depletion prompted us to examine its potential impact on chromosome segregation. For this, we conducted time-lapse imaging of oocytes expressing GFP-tagged tubulin and mCherry-tagged H2B, with and without BAF-1^{BAF} (Fig. 3 C). In both conditions, chromosomes aligned at the spindle equator on a tight metaphase plate during metaphase I. Throughout anaphase I, the segregating chromosomes maintained a compact arrangement, showing no signs of mis-segregation in both control and BAF-1^{BAF}–depleted oocytes. On the other hand, chromosome segregation was noticeably faster and resulted in a significantly increased distance between the two segregating chromosomal sets in the absence of BAF-1^{BAF} compared with control oocytes (Fig. 3 D). Since the overall chromosome structure and condensation, and the meiosis I spindle organization appeared normal in the absence of BAF-1^{BAF} (Fig. S2, F and G), our results suggest that the integrity of the interkinetic envelope impacts the normal pace and extent of chromosome segregation in *C. elegans* oocytes.

Since the complete depletion of BAF-1^{BAF} resulted in the formation of a highly fenestrated interkinetic envelope with significantly reduced membrane content, we next investigated whether over-recruiting BAF-1^{BAF} on chromosomes would have the opposite effect. To test this, we depleted the VRK-1^{VRK1} kinase (vaccinia related kinase), which phosphorylates BAF-1^{BAF} at the mitotic entry to promote its detachment from chromatin—an event essential for efficient NEBD (Fig. 4 A) (Gorjánácz et al., 2007). In the absence of VRK-1^{VRK1} during mitosis, BAF-1^{BAF} remains permanently bound to chromatin, leading to defects in NEBD and nuclear envelope reformation after mitosis, with excess membranes forming around chromosomes (Asencio et al., 2012; Gorjánácz et al., 2007). First, we verified the presence of VRK-1^{VRK1} at the surface of oocyte chromosomes during interkinesis (Fig. 4 B). As in mitosis, depleting VRK-1^{VRK1} led to an excess of BAF-1^{BAF} and LEM-2$^{LEMD2/3}$ on both chromosomal sets during interkinesis (Fig. 4, C and D). This suggests that VRK-1^{VRK-1} is at least partially responsible for the asymmetric localization of both proteins on chromosomes during interkinesis. Moreover, in the absence of VRK-1^{VRK1}, this overaccumulation of BAF-1^{BAF} and LEM-2$^{LEMD2/3}$ on chromosomes was accompanied by their noticeable stretching during segregation, which is reminiscent of the phenotype observed during mitosis in the same condition (Fig. 4 E). These defects of mitotic chromosome segregation have previously been attributed to the excess of membranes that surround them in the absence of VRK-1^{VRK-1} (Gorjánácz et al., 2007). To investigate whether membrane

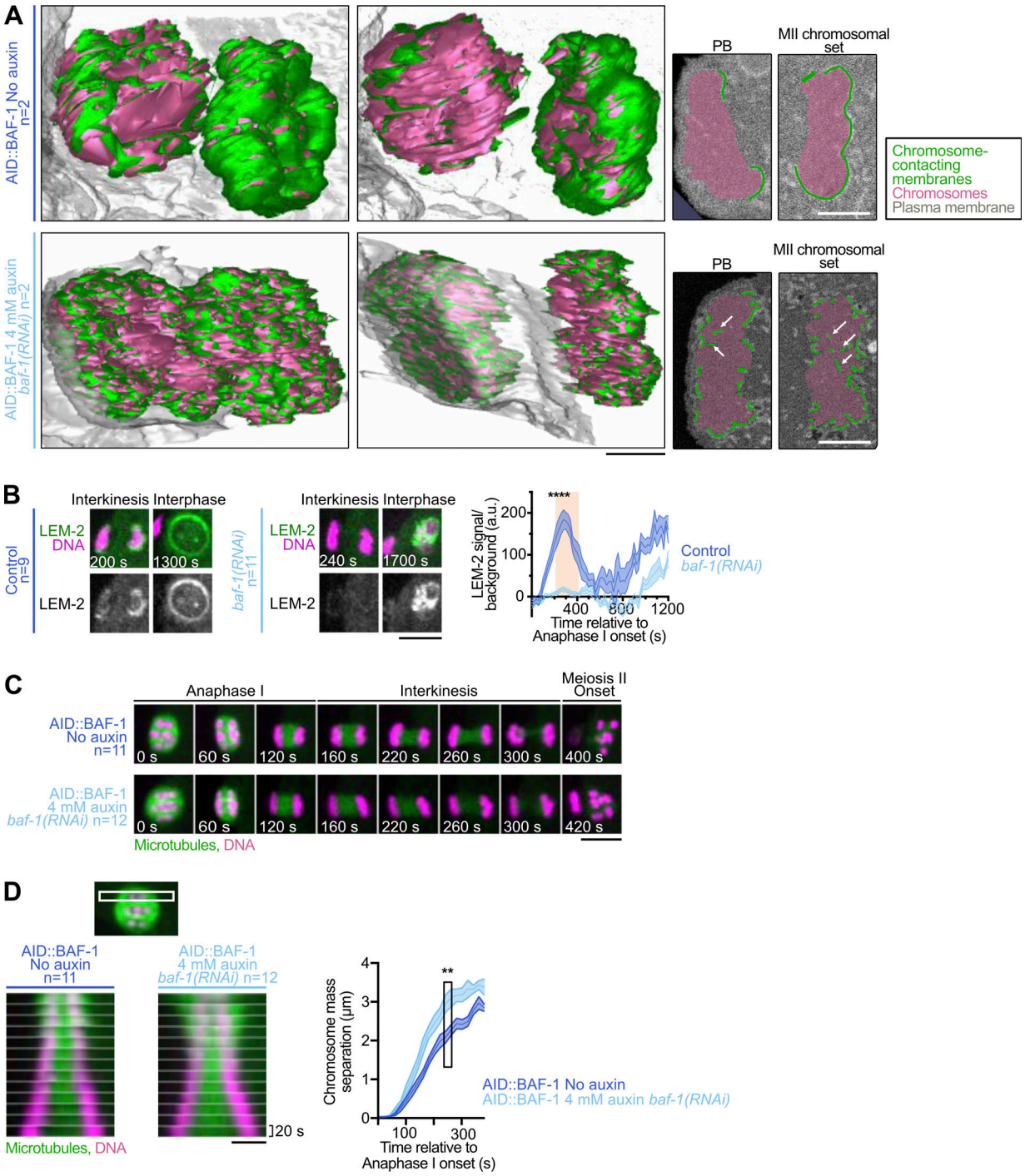

Figure 3. **BAF-1^{BAF} is essential for the integrity of the interkinetic envelope, for INM protein localization, and for normal chromosome segregation.** **(A)** Left: Three-dimensional reconstructions centered on chromosomes of a mid-interkinesis control oocyte (AID::BAF-1^{BAF}, No auxin) (top) and a mid-interkinesis BAF-1^{BAF}–depleted oocyte (AID::BAF-1^{BAF}, 4 mM auxin, *baf-1(RNAi)*) (bottom) viewed from two different angles. Scale bar, 1 µm. Right: two-dimensional single sections of two ROIs centered on each chromosomal set. Chromosomes in magenta, membranes in contact with chromosomes in green, and plasma membrane in gray. White arrows indicate membrane fragments within the chromosomal sets in the absence of BAF-1^{BAF}. Scale bar, 1 µm. **(B)** Left: Representative time-lapse images centered on chromosomes of oocytes expressing mCherry::H2B (magenta) and GFP::LEM-2$^{LEMD2/3}$ (green) during interkinesis and interphase in the indicated conditions. Timings indicated at the bottom left corners of images are from anaphase I onset. Scale bar, 5 µm. Right: Quantification of the normalized GFP::LEM-2$^{LEMD2/3}$ integrated intensity over time from anaphase I onset to interphase for the MII chromosomal set. Control in dark blue, *baf-1(RNAi)* in light blue. Error bars correspond to the standard error of the mean. The orange box indicates interkinesis. Mann-Whitney test on the mean value of GFP::LEM-2$^{LEMD2/3}$ intensity in interkinesis (****P < 0.0001). **(C)** Representative time-lapse images centered on chromosomes of oocytes expressing GFP::TBA-2$^{\alpha\text{-tubulin}}$ (green) and mCherry::HIS-11^{H2B} (magenta) during meiosis I in the indicated conditions. Timings indicated at the bottom left corners of images are from anaphase I onset. Scale bar, 5 µm. **(D)** Left: Kymographs showing a pair of segregating chromosomes in GFP::TBA-2$^{\alpha\text{-tubulin}}$ (green) and mCherry::HIS-11^{H2B} (magenta)–expressing oocytes from anaphase I onset in the indicated conditions. Scale bar, 5 µm. Right: Quantification of the distance

between the two sets of segregating chromosomes over time from anaphase I onset in control oocytes (dark blue) and BAF-1^{BAF}–depleted oocytes (light blue). Error bars correspond to the standard error of the mean. Mann–Whitney test on the mean distance between the segregating chromosomal sets during interkinesis in both conditions (**P < 0.01).

hyper-recruitment was responsible for chromosome stretching during interkinesis in VRK-1^{VRK1}–depleted oocytes, we conducted SBF-SEM followed by 3D reconstruction (Fig. 4 F). Surprisingly, although this approach confirmed the stretched chromosome phenotype, the density of membranes at the chromosomal surface was significantly reduced. In control oocytes, the total membrane length in contact with chromosomes was 325.24 µm compared with 199.51 µm in the absence of VRK-1^{VRK-1}. Thus, the chromosomal stretching observed in the absence of VRK-1^{VRK1} is likely due to a function separate from its role in interkinetic envelope assembly. Furthermore, the interkinetic envelope appeared highly fenestrated, similar to the phenotype observed in BAF-1^{BAF}–depleted oocytes. Thus, our results demonstrate that both depletion and over-recruitment of BAF-1^{BAF} on chromosomes lead to a similar reduction in membrane density and a highly fenestrated appearance at the chromosome surface during interkinesis. Overall, these findings underscore the critical role of BAF-1^{BAF}, whose chromosomal levels must be tightly regulated to ensure the proper assembly of the interkinetic envelope.

MEL-28^{ELYS} is essential for membrane recruitment on the chromosomal surface

We next sought to determine the origin of the double membranes that form the interkinetic envelope. In addition to BAF, nuclear envelope reformation at the end of mitosis requires the nucleoporin ELYS (Franz et al., 2007; Galy et al., 2006; Rasala et al., 2006). ELYS is a member of the "Y" nuclear pore subcomplex, which is essential for post-mitotic NPC reassembly and nuclear envelope integrity (Harel et al., 2003; Walther et al., 2003). In *C. elegans*, the orthologous protein MEL-28^{ELYS} is essential for nuclear envelope formation and function in embryos, and for chromosome segregation in oocytes (Fernandez and Piano, 2006; Galy et al., 2006; Gómez-Saldivar et al., 2016; Hattersley et al., 2016). During metaphase I in *C. elegans* oocytes, MEL-28^{ELYS} partially colocalizes with kinetochore cup-like structures on the surface of chromosomes, where it serves as a docking site for the catalytic subunit of protein phosphatase 1 (PP1c) (Bellutti et al., 2024; Hattersley et al., 2016). In anaphase I, the localization of MEL-28^{ELYS} spread over chromosomes, while also maintaining colocalization with the interkinetic envelope on both chromosomal sets (Fig. 5 A). At this stage, PP1c orchestrates kinetochore disassembly, a critical process for proper chromosome segregation (Hattersley et al., 2016). To explore the potential involvement of MEL-28^{ELYS} in interkinetic envelope assembly and double membrane recruitment, we performed SBF-SEM following RNAi-mediated depletion of MEL-28^{ELYS}. In line with previous findings, in the absence of MEL-28^{ELYS}, chromosomes within each chromosomal set were not as tightly grouped as compared with controls during anaphase I (Fig. 5 B, Fig. S3 A, and Video 7). Furthermore, physical segregation of the two chromosomal sets aborted rapidly after anaphase onset leading to a shorter separation distance compared with control oocytes at the same stage. Thus, to confirm that MEL-28^{ELYS}–depleted oocytes had reached interkinesis at the time of chemical fixation, we used time-lapse microscopy to capture their dynamics before proceeding with fixation and SBF-SEM (Fig. 5, B and C; Fig. S3, B and C; and Video 8). After segmentation and 3D reconstruction, we observed a drastic reduction in double membranes on the outer surface of chromosomes in MEL-28^{ELYS}–depleted oocytes compared with controls (total membrane length in contact with chromosomes in control oocytes was 317.53 µm versus 17.58 µm in the absence of MEL-28^{ELYS}). Upon segmentation and reconstruction of the other membrane compartments surrounding the segregating chromosomes (vesicles, mitochondria, and ER), we observed the expected meiotic spindle organelle exclusion zone around chromosomes in control oocytes (Fig. 5 D, Fig. S3 C, and Video 8) (Albertson and Thomson, 1993). However, in the absence of MEL-28^{ELYS}, the organelle exclusion zone was notably wider. Furthermore, this zone encompassed numerous unidentified small membrane fragments that surrounded the chromosomes but did not directly contact them—both features not observed in control oocytes. Thus, MEL-28^{ELYS} is required for interkinetic envelope assembly.

We hypothesized that the expanded organelle exclusion zone and the deficiencies in interkinetic envelope assembly in the absence of MEL-28^{ELYS} might, at least in part, result from the abnormal persistence of spindle pole microtubules throughout anaphase and interkinesis (Fig. 5 B) (Hattersley et al., 2016). These ectopic spindle pole microtubules could potentially act as a physical barrier, preventing membrane recruitment on the surface of chromosomes. To test this hypothesis, we compared the intensity of GFP::LEM-2$^{LEMD2/3}$ around chromosomes during interkinesis in the absence of MEL-28^{ELYS}, with and without microtubule depolymerization induced by nocodazole treatment (Fig. 5, E and F; and Fig. S3 D). As expected, GFP::LEM-2$^{LEMD2/3}$ was nearly absent from the surface of both chromosomal sets in the absence of MEL-28^{ELYS}. Importantly, this absence of GFP::LEM-2$^{LEMD2/3}$ was not attributed to the delocalization of BAF-1^{BAF}, which remained properly localized on the MII chromosomal set in the absence of MEL-28^{ELYS} (Fig. S3 E). Furthermore, upon microtubule depolymerization induced by nocodazole, GFP::LEM-2$^{LEMD2/3}$ levels on the MII chromosomal set were partially restored, reaching approximately half of the levels observed in control oocytes. Therefore, microtubule depolymerization can partially ameliorate the defects in interkinetic envelope assembly induced by MEL-28^{ELYS} depletion. During post-mitotic nuclear envelope reformation, ER sheets are enlisted at the chromosome surface to serve as a membrane source (Anderson and Hetzer, 2008; Anderson et al., 2009; Barger et al., 2022; Deolal et al., 2024; Haraguchi et al., 2001; Otsuka et al., 2018). Our findings collectively propose a distinct mechanism for interkinetic envelope assembly, implicating the MEL-

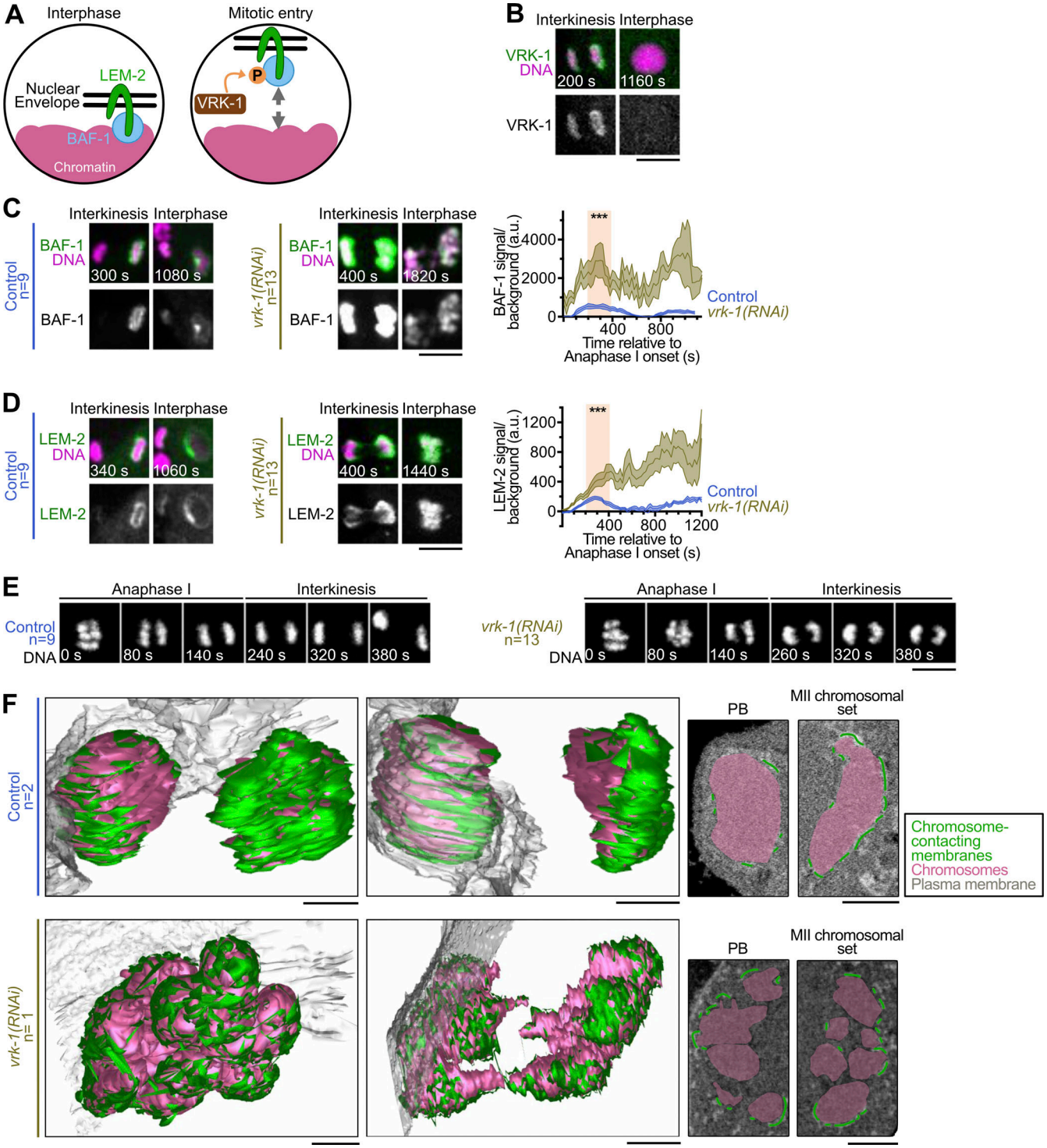

Figure 4. **VRK-1^{VRK} is essential for regulating BAF-1^{BAF} and LEM-2$^{LEMD2/3}$ recruitment and for the integrity of the interkinetic envelope. (A)** Left: Schematics of BAF-1^{BAF} and LEM-2$^{LEMD2/3}$ localization in interphase. Right: At mitotic entry, VRK-1^{VRK1} phosphorylates BAF-1^{BAF} and disrupts its chromatin binding. **(B)** Representative images of an ROI centered around chromosomes from oocytes expressing GFP::H2B and VRK-1^{VRK1}::mCherry (n = 12) during interkinesis and interphase. Timings indicated at the bottom left corner of images are from anaphase I onset. Scale bar, 5 µm. **(C and D)** Left: Representative time-lapse images centered on chromosomes of oocytes expressing mCherry::H2B (magenta) and (C) GFP::BAF-1^{BAF} or (D) GFP::LEM-2$^{LEMD2/3}$ (green) during interkinesis and interphase in the indicated conditions. Timings indicated at the bottom left corners of images are from anaphase I onset. Scale bar, 5 µm. Right: Quantification of the normalized GFP::LEM-2$^{LEMD2/3}$ integrated intensity over time from anaphase I onset to interphase for the MII chromosomal set. Control in dark blue and *vrk-1(RNAi)* in light brown. Error bars correspond to the standard error of the mean. The orange box indicates interkinesis. Mann–Whitney test on the mean value of GFP::LEM-2$^{LEMD2/3}$ intensity in interkinesis (***P < 0.001). **(E)** Representative time-lapse images centered on chromosomes of oocytes expressing mCherry::H2B (gray) during anaphase I and interkinesis in the indicated conditions. Timings indicated at the bottom left corners of images are from anaphase I onset. Scale bar, 5 µm. **(F)** Left: Three-dimensional reconstructions centered on chromosomes of a control oocyte (top) and a VRK-1^{VRK1}–depleted

oocyte (bottom) viewed from two different angles. Scale bar, 1 µm. Right: Two-dimensional single sections of two ROIs centered on each chromosomal set. Chromosomes in magenta, membranes in contact with chromosomes in green, and plasma membrane in gray. Scale bar, 1 µm. The same control oocyte is displayed in Fig. 5 C.

28^{ELYS}–mediated accumulation of small unidentified membrane fragments on the surface of the chromosomal sets. Moreover, this process is contingent, at least to some extent, on the rapid disassembly of spindle pole microtubules, a process that occurs early during anaphase in control oocytes but is strongly delayed in the absence of MEL-28^{ELYS} (Hattersley et al., 2016).

The interkinetic envelope contains nucleoporins but not NPCs

MEL-28^{ELYS} is essential for post-mitotic nuclear pore complex reformation (Franz et al., 2007; Galy et al., 2006). At the mitotic exit, MEL-28^{ELYS} binds to chromatin and recruits other nuclear pore components that form six to eight protein modules, the NPC subcomplexes (Fernandez-Martinez and Rout, 2021; Huang et al., 2023; Lin and Hoelz, 2019). In *C. elegans*, the NPC comprises 28 identified nuclear pore proteins (NPPs) distributed into six subcomplexes: the cytoplasmic and nucleoplasmic rings (also known as the "Y-complex," which contains MEL-28^{ELYS}), the inner ring, the transmembrane nucleoporins, the central channel, the nuclear basket, and the cytoplasmic filaments (Cohen-Fix and Askjaer, 2017). In addition to MEL-28^{ELYS}, previous work revealed the presence of NPP-6^{NUP160}, a Y-complex nucleoporin, on the surface of the segregating chromosomal sets during anaphase I in *C. elegans* oocytes (Penfield et al., 2020).

Using transgenic and endogenously fluorescently tagged *C. elegans* strains, we analyzed the interkinetic localization of 18 nucleoporins (of the 28 *C. elegans* NPPs) that systematically represent all major subcomplexes of the NPC (Fig. 6). We first validated NPP-6^{NUP160} localization and observed a comparable chromosomal pattern for other Y-complex constituents, including NPP-2^{NUP85}, NPP-5^{NUP107}, NPP-15^{NUP133}, NPP-18^{SEH1}, and NPP-20^{SEC13R}. The inner ring complex lines the inner part of the NPC. We detected the presence of the inner ring component NPP-19^{NUP35}, but not NPP-13^{NUP93} or NPP-8^{NUP155}, at the outer surface of the MII chromosomal set. The central channel is formed by nucleoporins that contain phenylalanine (F) and glycine (G) repeats essential for establishing nuclear pore permeability. We could not detect the presence of the central channel nucleoporin NPP-1^{NUP54}, and NPP-11^{NUP62} predominantly localized between the two sets of segregating chromosomes in a region corresponding to the anaphase I central spindle. The nuclear basket forms the nucleoplasmic side of the NPC. We found nuclear basket NPP-7^{NUP153} distributed across the entire surface of both chromosome sets, whereas NPP-21^{TPR} was absent. On the other side of the NPC, the cytoplasmic filaments include the nucleoporin NPP-24^{NUP88}, which like NPP-11^{NUP62}, was concentrated in the central spindle region during interkinesis. Finally, transmembrane nucleoporins NPP-12^{NUP210} and NPP-25^{TMEM33}, but not NPP-22^{NDC1}, were present on the outer surface of the MII chromosomal set. In summary, our investigation revealed the presence of all examined Y-complex nucleoporins, along with specifically NPP-19^{NUP35} (inner ring), NPP-7^{NUP153} (nuclear basket), NPP-12^{NUP210} and NPP-25^{TMEM33} (transmembrane), distributed across the entire surface of both chromosomal sets and/or asymmetrically at the interkinetic envelope. That is, nucleoporins within the same NPC subcomplex were not necessarily co-recruited to the interkinetic envelope, preventing the formation of functional subcomplexes or NPCs. In agreement, despite the presence of various nucleoporins and in alignment with prior observations (Penfield et al., 2020), both our SBF-SEM and electron tomography analyses consistently indicated the absence of nuclear pores within the interkinetic envelope. Overall, while lacking nuclear pores, the presence of nucleoporins hints at their potential engagement in unconventional functions during interkinetic envelope assembly.

Nucleoporins with membrane binding domains could contribute to interkinetic envelope integrity

We next tested the role of nucleoporins in interkinetic envelope assembly. Interestingly, aside from the two transmembrane proteins NPP-12^{NUP210} and NPP-25^{TMEM33}, responsible for post-mitotic NPC anchoring in nuclear membranes and found at the interkinetic envelope, several nucleoporins identified in the interkinetic envelope are predicted to possess domains capable of folding as amphipathic helices, which can bind to membranes (Cohen et al., 2003; Floch et al., 2015; Greber et al., 1990; Hamed and Antonin, 2021; Vollmer et al., 2012, 2015). These included Y-complex nucleoporins NPP-6^{NUP160} and NPP-15^{NUP133}, inner ring component NPP-19^{NUP35}, and nuclear basket protein NPP-7^{NUP153}. We systematically depleted each of these six nucleoporins by RNAi and analyzed interkinetic envelope integrity by time-lapse imaging using GFP::LEM-2$^{LEMD2/3}$ intensity as a proxy (Fig. 7, A and B; Fig. S4; and Video 9). Individual depletion of all six nucleoporins led to a mild but significant decrease in GFP::LEM-2$^{LEMD2/3}$ intensity at the chromosomal surface during interkinesis. Importantly, depleting the inner ring nucleoporin NPP-8^{NUP155}, which we did not find localized at the interkinetic envelope, exhibited no discernible effect on GFP::LEM-2$^{LEMD2/3}$ intensity (Fig. S5 A). In line with the mild decrease in LEM-2$^{LEMD2/3}$ intensity, none of the individual nucleoporin depletions caused chromosome segregation defects (Fig. S5 B). To determine whether depleting multiple nucleoporins would have a stronger effect, we systematically co-depleted the six nucleoporins in pairs. While all co-depletions consistently exacerbated the delocalization of GFP::LEM-2$^{LEMD2/3}$ from the chromosome surface compared with single depletions, none resulted in its complete absence (Fig. 7 B and Fig. S5 C). We were unable to assess the effect of the simultaneous depletion of NPP-12^{NUP210} and NPP-19^{NUP35}, as it caused the failure of oocyte NEBD and blocked meiotic divisions. Overall, our results suggest that nucleoporins function in parallel for membrane recruitment, and their roles in interkinetic envelope assembly are at least partially redundant.

Finally, we tested whether this network of nucleoporins was hierarchically positioned downstream of MEL-28^{ELYS}, akin to

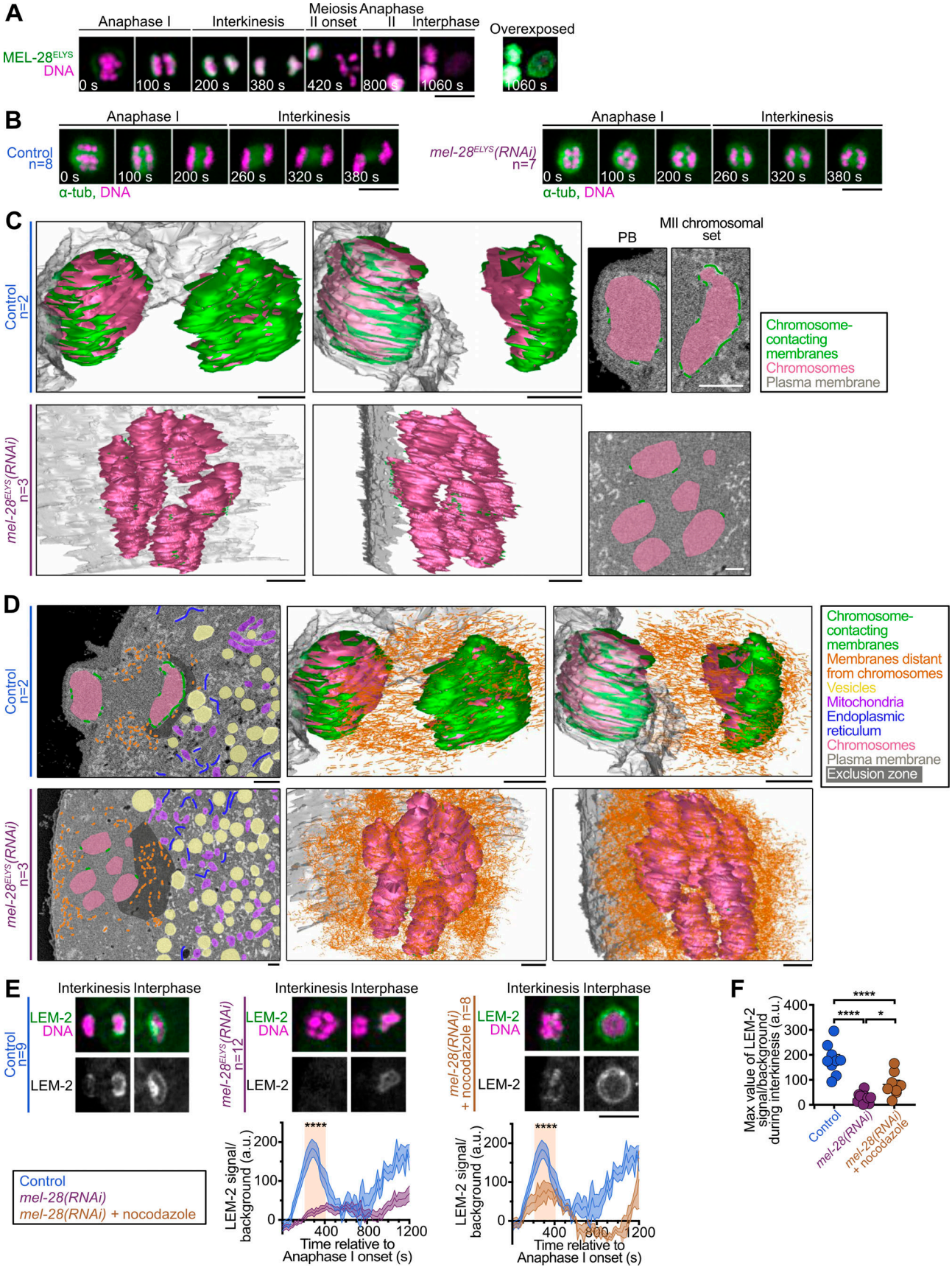

Figure 5. **MEL-28^{ELYS} is essential for interkinetic envelope integrity and membrane recruitment. (A)** Representative time-lapse images centered on chromosomes of oocytes (n = 8) expressing mCherry::H2B (magenta) and GFP::MEL-28^{ELYS} (green) during meiosis I and II. Timings indicated at the bottom left

corners of images are from anaphase I onset. Scale bar, 5 µm. **(B)** Representative time-lapse images centered on chromosomes of oocytes expressing mCherry::H2B (magenta) and GFP::TBA-2$^{\alpha\text{-tubulin}}$ (green) and mCherry::HIS-11^{H2B} (green) during anaphase I and interkinesis in the indicated conditions. Timings indicated at the bottom left corners of images are from anaphase I onset. Scale bar, 5 µm **(C)** Left: Three-dimensional reconstructions centered on chromosomes of a control oocyte (top) and a MEL-28^{ELYS}–depleted oocyte (bottom) viewed from two different angles. Scale bar, 1 µm. Right: Two-dimensional single sections of ROIs centered on each chromosomal set. Chromosomes in magenta, membranes in contact with chromosomes in green, and plasma membrane in gray. Scale bar, 1 µm. The same control oocyte is displayed in Fig. 4 F. **(D)** Left: Two-dimensional single sections of ROI centered on each chromosomal set of a control oocyte (top) and a MEL-28^{ELYS}–depleted oocyte (bottom). Scale bar, 1 µm. Right: Three-dimensional reconstructions centered on chromosomes viewed from two different angles. Scale bar, 1 µm. Chromosomes in magenta, membranes in contact with chromosomes in green, membranes distant from chromosomes in orange, vesicles in yellow, mitochondria in purple, endoplasmic reticulum in blue, and plasma membrane in gray. Scale bar, 1 µm. **(E)** Top: Representative time-lapse images centered on chromosomes of oocytes expressing mCherry::H2B (magenta) and GFP::LEM-2$^{LEMD2/3}$ (green) during interkinesis and interphase in the indicated conditions. Timings indicated at the bottom left corners of images are from anaphase I onset. Scale bar, 5 µm. Bottom: Quantification of the normalized GFP::LEM-2$^{LEMD2/3}$ integrated intensity over time from anaphase I onset to interphase for the MII chromosomal set. Control in dark blue, *mel-28(RNAi)* in purple, *mel-28(RNAi)* treated with 100 ng/µl nocodazole in brown. Error bars correspond to the standard error of the mean. The orange box indicates interkinesis. Mann–Whitney test on the mean value of GFP::LEM-2$^{LEMD2/3}$ intensity in interkinesis (****P < 0.0001). **(F)** Quantifications of the maximal mean value of GFP::LEM-2$^{LEMD2/3}$ intensity in interkinesis normalized over background in the indicated conditions. One-way ANOVA test (****P < 0.0001, *P < 0,05).

during post-mitotic NPC reformation (Franz et al., 2007; Galy et al., 2006). For this, we analyzed the localizations of GFP-tagged NPP-6^{NUP160}, NPP-15^{NUP133}, NPP-25^{TMEM33}, NPP-12^{NUP210}, NPP-19^{NUP35}, and NPP-7^{NUP153} in oocytes during interkinesis upon MEL-28^{ELYS} depletion by RNAi (Fig. 8 and Video 10). The intensities of all six nucleoporins on the chromosome surface were markedly reduced in the absence of MEL-28^{ELYS} during interkinesis, with NPP-6^{NUP160}, NPP-7^{NUP153}, and NPP-19^{NUP35} absent from chromosomes. These results indicated that chromatin-bound MEL-28^{ELYS} serves as a precursor to a network of nucleoporins including NPP-6^{NUP160}, NPP-7^{NUP153}, NPP-12^{NUP210}, NPP-15^{NUP133}, NPP-19^{NUP35}, and NPP-25^{TMEM33}. This network could interact with membranes and mediate their recruitment to the chromosomal surface, thus promoting interkinetic envelope assembly.

Discussion

The suppression of most interphasic events during interkinesis in oocytes, including chromosome decondensation and genome replication, led to the widely accepted assumption that the nuclear envelope does not reassemble during this short transition phase between meiosis I and II (Gerhart et al., 1984; Lénárt and Ellenberg, 2003; Nakajo et al., 2000; Nebreda and Ferby, 2000). However, by combining electron microscopy and time lapse imaging in *C. elegans* oocytes during interkinesis, we found that an interkinetic envelope transiently forms around condensed chromosomes at this stage. Although this envelope is not nuclear as it does not compartmentalize the genome, it nevertheless shares several features with the nuclear envelope, including its double-membrane structure and protein composition of the inner layer. It also displays distinct and surprising differences from nuclear envelopes.

A striking feature of the interkinetic envelope is its lack of continuity with the ER. During post-mitotic nuclear envelope reformation, ER membranes are recruited at chromosome surfaces to regenerate nuclear envelope membranes (Anderson and Hetzer, 2008; Anderson et al., 2009; Deolal et al., 2024; Haraguchi et al., 2001; Otsuka et al., 2018). Proteins can then translocate seamlessly from the ER to the ONM, resulting in partial sharing of protein composition between these structures (Deolal et al., 2024). In contrast, the lack of continuity between the interkinetic envelope and the meiotic ER likely explains the apparent absence of ONM protein within the interkinetic envelope. The reasons for the absence of a junction between the interkinetic envelope and the ER remain unclear. There may be an unknown physical barrier that prevents the interkinetic envelope from incorporating ER-derived membranes. Alternatively, missing components within the interkinetic envelope could inhibit the fusion of these two structures. Notably, despite being discovered decades ago, the mechanism for junction formation between the ER and the nuclear envelope in mitotic cells remains unknown (Watson, 1955; Whaley et al., 1960). Further investigation will be required to uncover the molecular mechanism underlying this unique feature of the interkinetic envelope.

In the absence of physical contact with the ER, we found that a population of small membrane fragments, the origin and identity of which are at present unclear, positioned near chromosomes, seemed to participate in interkinetic envelope assembly. We suspect that these small membrane fragments could originate from nuclear envelope remnants following NEBD of the diakinesis oocyte (Lénárt and Ellenberg, 2003). Our functional analysis suggests that MEL-28^{ELYS} acts as an upstream regulator of these fragments. In its absence, the small membrane fragments concentrated around the segregating chromosomes but did not contact them to assemble an envelope at their surface.

We identified two complementary functions for MEL-28^{ELYS} at the interkinetic envelope. First, we found that in absence of MEL-28^{ELYS}, the observed small membrane fragments were positioned further away from chromosomes, likely caused by persistent ectopic spindle poles during anaphase I in absence of MEL-28^{ELYS} (Hattersley et al., 2016). Second, we found that several nucleoporins bearing potential membrane-binding domains were recruited downstream of MEL-28^{ELYS} to the interkinetic envelope. Our results suggest that these nucleoporins could recruit membranes necessary for interkinetic envelope assembly at the surface of chromosomes. The role of MEL-28^{ELYS} in nucleoporin recruitment to the interkinetic envelope could be direct or indirect. Indeed, during post-mitotic nuclear envelope reassembly, a key initial event is the dephosphorylation of

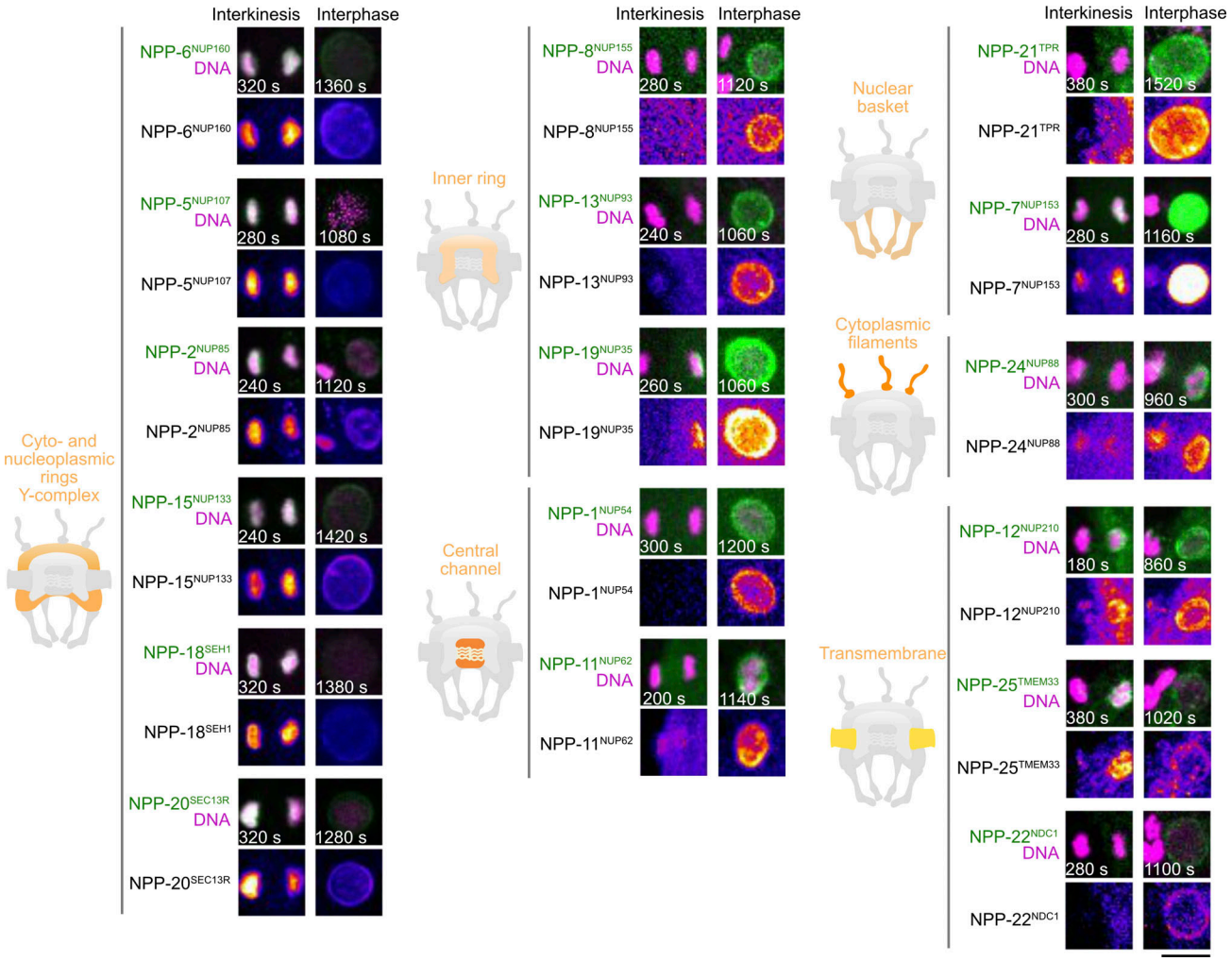

Figure 6. **The interkinetic envelope contains nucleoporins but not NPCs.** Localization of NPPs during interkinesis and interphase grouped by theoretical subcomplexes. Left: Schematics of each subcomplex localization at the NPC. Right: Representative images of a region of interest centered around chromosomes of oocytes expressing mCherry::H2B and either GFP-tagged NPP-2^{NUP85} (n = 10), NPP-5^{NUP107} (n = 7), NPP-6^{NUP160} (n = 6), NPP-15^{NUP133} (n = 10), NPP-18^{SEH1} (n = 5), NPP-20^{SEC13R} (n = 10), NPP-13^{NUP93} (n = 6), NPP-19^{NUP35} (n = 10), NPP-12^{NUP210} (n = 7), NPP-22^{NDC1}, NPP-25^{TMEM33} (n = 7), NPP-1^{NUP54} (n = 15), NPP-11^{NUP62} (n = 11), NPP-7^{NUP153} (n = 15), NPP-21^{TPR} (n = 7), NPP-24^{NUP88} (n = 7), or mCherry-tagged NPP-8^{NUP155} (n = 14) (green) during interkinesis and interphase. Timings indicated at the bottom left corner of images are from anaphase I onset. Scale bar, 5 µm.

nuclear envelope components, including lamins and nucleoporins, by protein phosphatases PP1 or PP2A (Hattersley et al., 2016; Mehsen et al., 2018; Steen et al., 2000). During meiosis I in *C. elegans* oocytes, MEL-28^{ELYS} is responsible for the docking of the catalytic subunit of PP1 on chromosomes (Hattersley et al., 2016). Thus, PP1 docked by MEL-28^{ELYS} on chromosomes could regulate the phosphorylation state of components essential for interkinetic envelope assembly, which would in turn promote their chromosomal recruitment.

The potential link we establish between nucleoporins bearing membrane-binding domains and interkinetic envelope assembly pertains to a non-conventional role of these nucleoporins outside their canonical function in the formation of nuclear pores. We indeed observed a complete lack of nuclear pores in the interkinetic envelope despite the presence of these nucleoporins. Consistent with this observation, we found that nucleoporins that normally belong to the same NPC sub-complex were not co-recruited to the interkinetic envelope. We indeed found that NPP-21^{TPR} was absent despite the presence of NPP-7^{NUP153}, which is both necessary and sufficient for its recruitment to NPCs during interphase (Hase and Cordes, 2003; Walther et al., 2001). While the recruitment of NPP-8^{NUP155} and NPP-19^{NUP35} are interdependent at NPCs, we observed NPP-19^{NUP35} localized in the absence of NPP-8^{NUP155} at the interkinetic envelope (Ródenas et al., 2009). Moreover, nucleoporins essential for nuclear pore assembly (i.e., NPP-8^{NUP155}) were even missing from the interkinetic envelope (Franz et al., 2005). The lack of NPCs in the interkinetic envelope is not surprising in light of their normal function in regulating transport between the physically segregated nucleoplasm and cytoplasm during interphase. The interkinetic envelope is a transient structure that only exists during the short transition period between meiosis I and II, and unlike the nuclear envelope, the interkinetic envelope never seals completely. During this stage, the condensed

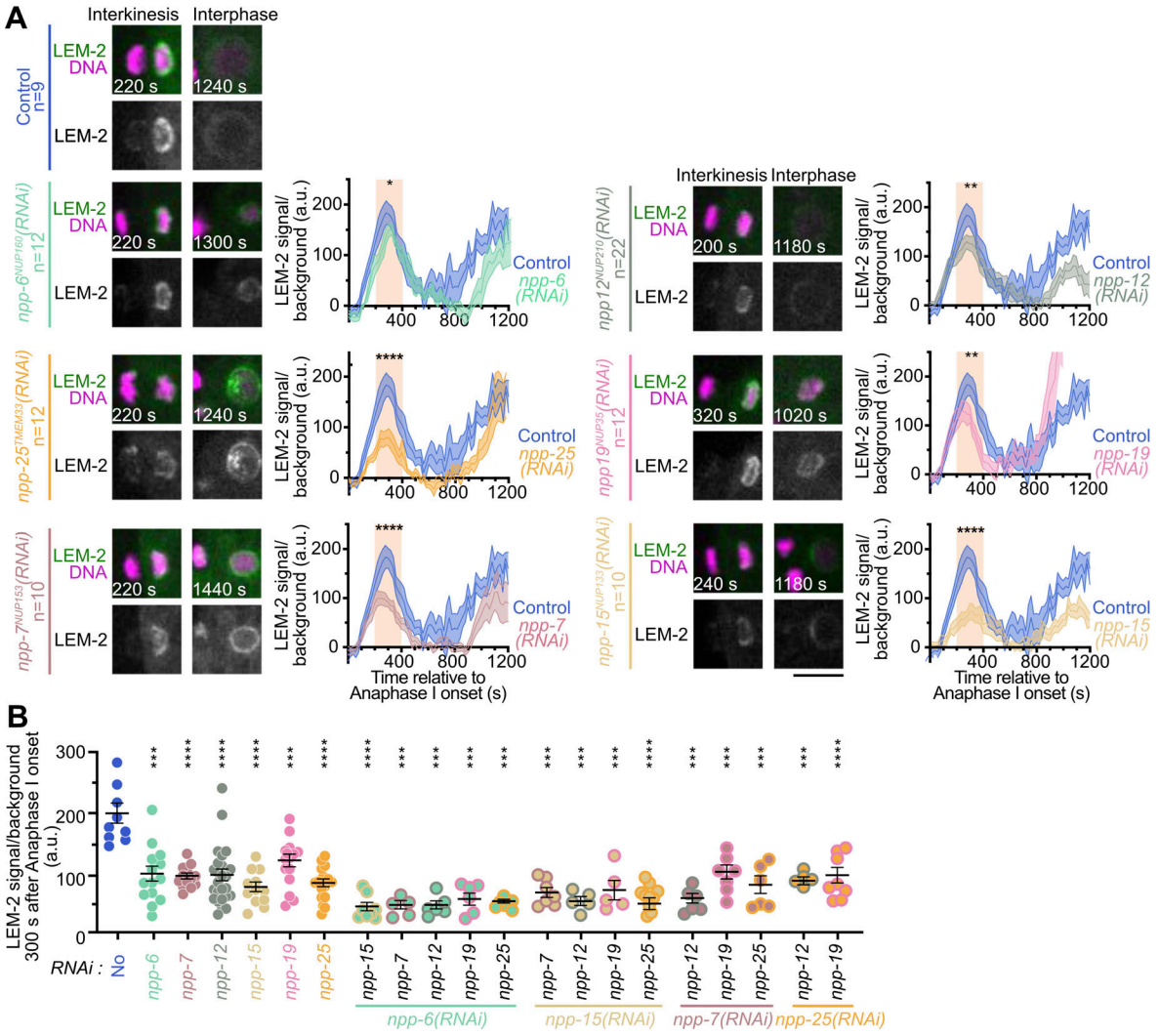

Figure 7. **Nucleoporins with a membrane-binding domain could contribute to interkinetic envelope integrity. (A)** Left: Representative time-lapse images centered on chromosomes of oocytes expressing mCherry::H2B (magenta) and GFP::LEM-2$^{LEMD2/3}$ (green) during interkinesis and interphase in the indicated conditions. Timings indicated at the bottom left corners of images are from anaphase I onset. Scale bar, 5 µm. Right: Quantification of the normalized GFP::LEM-2$^{LEMD2/3}$ integrated intensity over time from anaphase I onset to interphase for the MII chromosomal set. Control in dark blue, *npp-6^{NUP160}(RNAi)* in turquoise, *npp-25^{TMEM33}(RNAi)* in dark orange, *npp-15^{NUP133}(RNAi)* in light orange, *npp-12^{NUP210}(RNAi)* in gray, *npp-19^{NUP53}(RNAi)* in pink, and *npp-7^{NUP153} (RNAi)* in light brown. Error bars correspond to the standard error of the mean. The orange box indicates interkinesis. Mann–Whitney test on the mean value of GFP::LEM-2$^{LEMD2/3}$ intensity in interkinesis (*P < 0.05, **P < 0.01, ****P < 0.0001). **(B)** Quantification of the normalized GFP::LEM-2$^{LEMD2/3}$ intensity at 300 s after anaphase I onset in the indicated conditions. Mann–Whitney test (***P < 0.001 and ****P < 0.0001).

chromosomes are thus in contact with the cytoplasmic content, and can in theory freely exchange components.

Despite the lack of complete interkinetic envelope sealing, we found that the structural integrity of the interkinetic envelope is functionally important. In the absence of the chromatin-binding protein BAF-1^{BAF}, the interkinetic envelope was highly fenestrated and membrane fragments were observed between chromosomes of a given chromosomal set. This phenotype is reminiscent of the post-mitotic nuclear envelope defects, including envelope fragmentation and micronucleation, observed following BAF depletion in human tissue cultured cells and during *C. elegans* mitosis (Barger et al., 2023; Gorjánácz et al., 2007; Samwer et al., 2017). Recent studies have revealed that BAF not only plays a role in recruiting LEM-domain proteins for nuclear envelope assembly, as previously thought, but is also involved in DNA cross-bridging (Samwer et al., 2017). This function is carried out by BAF on chromosomes, where it creates a mechanically rigid surface of chromatin. This rigid chromatin surface restricts nuclear membranes to the chromosome surface and effectively prevents membrane fragmentation. Whether BAF-1^{BAF} functions by promoting DNA cross-bridging, by targeting LEM-domain proteins, or through a combination of both mechanisms during interkinetic envelope assembly remains unclear. However, several lines of evidence suggest that both mechanisms may be involved. First, the presence of membrane fragments within chromosomal sets in the absence of BAF-1^{BAF}—a phenotype never observed under normal conditions—implies that BAF-1^{BAF} may be crucial for excluding membranes

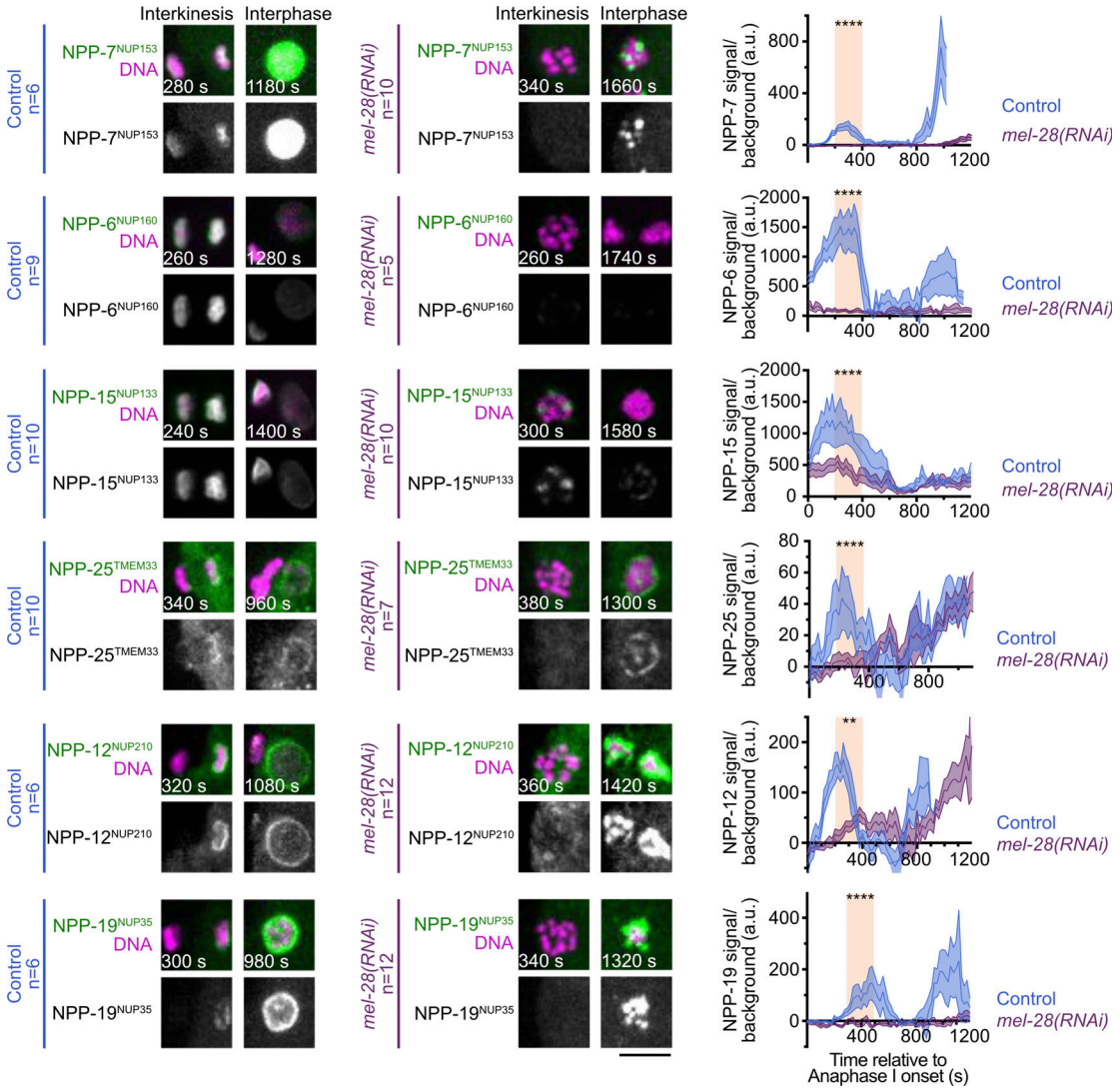

Figure 8. **Hierarchical relationships between MEL-28^{ELYS} and nucleoporins bearing a membrane-binding domain during interkinetic envelope assembly.** Left: Representative time-lapse images centered on chromosomes of oocytes expressing mCherry::H2B (magenta) and either GFP-tagged NPP-6^{NUP160}, NPP-15^{NUP133}, NPP-25^{TMEM33}, NPP-12^{NUP210}, NPP-19^{NUP35}, or NPP-7^{NUP153} (green) during interkinesis and interphase in the indicated conditions. Timings indicated at the bottom left corners of images are from anaphase I onset. Scale bar, 5 µm. Right: Quantification of the normalized GFP-tagged NPP-6^{NUP160}, NPP-15^{NUP133}, NPP-25^{TMEM33}, NPP-12^{NUP210}, NPP-19^{NUP35}, or NPP-7^{NUP153} integrated intensity over time from anaphase I onset to interphase for the MII chromosomal set. Control in dark blue and *mel-28(RNAi)* in purple. Error bars correspond to the standard error of the mean. The orange box indicates interkinesis. Mann–Whitney test on the mean value of GFP::LEM-2$^{LEMD2/3}$ intensity in interkinesis (**P < 0.01, ****P < 0.0001).

from the spaces between chromosomes, suggesting its role in DNA cross-bridging. Second, our finding that depleting VRK-1^{VRK1}, the kinase that negatively regulates BAF-1^{BAF} chromatin binding, produces the same fenestrated interkinetic envelope phenotype as BAF-1^{BAF} depletion but without interchromosomal membrane fragments, shows that these two phenotypes can be functionally separated. Furthermore, we found that VRK-1^{VRK1} and BAF-1^{BAF} depletion have opposite effects on LEM-domain protein chromosomal localization. Thus, our observation that both the absence and over-recruitment of LEM-2$^{LEMD2/3}$ is coupled to the same fenestrated interkinetic envelope phenotype suggests that precise regulation of LEM domain protein localization is an essential factor for proper interkinetic envelope assembly. A key question is the potential function of the interkinetic envelope. While it may simply result from chromosomes remaining permanently condensed and exposed in the absence of spindle microtubules during interkinesis—allowing the transient recruitment of some inner nuclear envelope components and associated membranes—our findings suggest that the interkinetic envelope could play an active role in meiotic chromosome segregation. In the absence of BAF-1^{BAF}, we observed fragmentation of the envelope, leading to accelerated and more extensive chromosome segregation compared to control oocytes. This suggests that the interkinetic envelope could act as a brake for meiotic chromosome segregation by mechanically constraining chromosomes and the pushing anaphase spindle. However, we believe that the observed phenotype may underestimate the true importance of the interkinetic envelope.

Indeed, upon depletion of BAF-1^{BAF}, although the interkinetic envelope becomes abnormally fenestrated, it still surrounds the surface of chromosomes, unlike the total absence of an envelope seen upon MEL-28^{ELYS} depletion. A striking observation is the abnormal spreading of chromosomes within each set in the absence of MEL-28^{ELYS}, suggesting that the interkinetic envelope may play a role in keeping each chromosomal set tightly clustered to prevent the mixing of PB and MII chromosomes during segregation. Unfortunately, the severe chromosome segregation defects resulting from the lack of PP1-mediated kinetochore disassembly during meiotic anaphase after MEL-28^{ELYS} depletion prevented us from selectively analyzing the contribution of the interkinetic envelope to chromosome segregation (Gómez-Saldivar et al., 2016; Hattersley et al., 2016). Thus far, we have been unable to recapitulate the complete absence of an interkinetic envelope, nor the chromosome segregation defects observed in the absence of MEL-28^{ELYS}, using other experimental perturbations. Understanding the true function of the interkinetic envelope in meiotic chromosome segregation will require further investigation.

The scarcity of research on interkinesis has left the existence of an interkinetic envelope in oocytes of species other than *C. elegans* largely unknown and will be an interesting avenue for future studies.

Materials and methods

Maintenance of *C. elegans* lines

The worm lines used in this study are listed in Table S1. The worms were maintained on plates containing nematode growth medium (NGM) agar seeded with OP50 *E. coli* bacteria at 23°C. All worms analyzed were hermaphrodites.

RNA interference

Double-stranded RNAs (dsRNAs) used in this study are listed in Table S2. They were synthesized using the primers and templates indicated in the same table. PCR products were purified (PCR purification kit; Qiagen) and used as templates for T3 and T7 transcription reactions (Megascript, #AM1334 for T7 and #AM1338 for T3; Invitrogen). The produced RNAs were purified (MEGAclear kit, #AM1908; Invitrogen) and then hybridized by incubation at 68°C for 10 min, followed by 37°C for 30 min. L4-stage hermaphrodites were injected with dsRNAs at the specified concentrations and incubated at 20°C for 44–48 h before imaging.

Auxin-induced degradation

The strain expressing endogenously tagged baf-1 (PHX2768) with an auxin-inducible degron (mAID) was first crossed with the strain CA1199, expressing a TIR1 transgene (*sun-1p::TIR1::mRuby::sun-1 3′UTR + Cbr-unc-119(+)*) (Zhang et al., 2015) under the control of the germline-specific sun-1 promoter and then with the GFP::TBA-2$^{\alpha\text{-tubulin}}$ and mCherry::H2B under the control of the germline-specific mex-5 promoter, -expressing worms from the strain JDU233. Full BAF-1 depletion was achieved by combining RNAi-mediated depletion of the *baf-1* mRNA and auxin-induced degradation of the BAF-1 protein. Briefly, 32 h after injection of dsRNA targeting *baf-1* in JDU647, worms were incubated for 16 h on NGM agar plates seeded with OP50 *E. coli* bacteria containing 4 mM auxin.

Oocyte time-lapse imaging

Adult worms were dissected in 5 µl of meiosis medium (0.5 mg/ml Inulin, 25 mM HEPES, 60% Leibovitz L-15 medium, and 20% fetal bovine serum). Imaging was conducted at 23°C using the CherryTemp temperature control system (CherryBiotech). All acquisitions were performed with a Nikon Ti-E inverted microscope, equipped with a CSU-X1 spinning disk confocal head (Yokogawa), an emission filter wheel, and a coolSNAP HQ2 CCD camera (Photometrics Scientific). Stage control and focus correction during acquisition were conducted using the PZ-2000 XYZ piezo motor from Applied Scientific Instrumentation. Movies were acquired with 2 × 2 binning using a Nikon CFI APO S 60x/NA1.4 oil immersion objective. For all movies, four Z-stack planes, separated by 2 µm, were acquired every 20 s. Acquisition parameters were controlled using Metamorph 7 software (RRID:SCR_002368; Molecular Devices). For nocodazole treatment, adult worms were dissected in a meiosis medium supplemented with 100 ng/µl nocodazole (#M1404; Sigma-Aldrich).

SBF-SEM

After dissecting worms in 5 µl of meiosis medium, oocytes were transferred and packed into nitrocellulose capillary tubes with an inner diameter of 200 µm (16706869; Leica Microsystems). The tube was sealed using the flat top edge of the scalpel. Oocytes enclosed in the capillary tubes were maintained on a glass slide in a droplet of meiosis medium and recorded by videomicroscopy under the spinning disc confocal microscope as described above. Once in interkinesis, 15 µl of fixative medium (1% glutaraldehyde, 2% formaldehyde in 1× PBS) was added to the 5 µl of meiosis medium containing the capillary tube. Then, each capillary containing an oocyte was transferred into a 1.5 ml Eppendorf tube containing 1 ml of fixative medium. The oocytes were subsequently incubated for 1 h at room temperature and kept at 4°C until further preparation (Deerinck et al., 2010). After three washes in 1× PBS, the oocytes were treated with 1% osmium tetroxide (OsO_4) and 1.5% potassium ferrocyanide in 1× PBS at 4°C for an hour. They were then incubated in a 1% thiocarbohydrazide solution in water for 20 min at room temperature. Subsequently, they were treated with 2% aqueous OsO_4 for 30 min at room temperature before an overnight incubation at 4°C in 1% uranyl acetate in water. The following day, the samples were subjected to Walton's lead aspartate block staining (Walton, 1979) and placed in an oven at 60°C for 30 min. The samples were then dehydrated in gradual ethanol concentrations (20%, 30%, 50%, 70%, 90%, and 100%) for 10 min each at room temperature on a wheel. The samples were infiltrated with a low-viscosity Agar resin (Agar Scientific Ltd.) at 30% for 1 h, then at 50% for 2 h, at 75% for 2 h, and finally at 100% overnight. The resin was then replaced and the samples were reincluded for 3 h before being mounted and polymerized for 18 h at 60°C. The samples, permeated with 100% resin, were embedded in a flat layer of resin and then polymerized at 60°C for 18 h. The

polymerized blocks were mounted on special aluminum pins for SBF-SEM imaging (FEI Microtome 8 mm SEM Stub; Agar Scientific), with a two-part silver epoxy conduction kit (190215; EMS). The samples mounted on aluminum pins were cut and inserted into a TeneoVS scanning electron microscope (Thermo Fisher Scientific). The acquisitions were carried out with a beam energy of 2 kV, 200 pA, in LowVac mode at 40 Pa, a pixel dwell time of 1 µs, and serial-sections of 30 nm and imaging was performed. The IMOD software (RRID:SCR_003297) was then used for stack reconstructions and segmentation (Kremer et al., 1996).

Immunofluorescence

10–15 adult worms were dissected in 3.5 µl of meiosis medium on poly-L-lysine–coated slides (1 mg/ml in PBS P-1524; Sigma-Aldrich). The slides were covered with a 12 × 12 mm coverslip and snap-frozen in liquid nitrogen. The oocytes were then fixed in 100% methanol for 20 min at −20°C. After two 10-min washes in 1× PBS, the oocytes were blocked in an antibody diluent solution (AbDil containing 4% bovine serum albumin and 0.1% Triton in PBS) for an hour at room temperature in a humid chamber. The samples were subsequently incubated overnight at 4°C in a primary antibody solution (Table S3). After two washes in AbDil, the samples were incubated for an hour at room temperature with 1:100 secondary antibodies. After two washes in AbDil, DNA was counterstained with 2 µg/ml Hoechst 33342 for 10 min. They were then washed twice with 1× PBS + 0.1% Triton X-100 and once with 1× PBS. Samples were mounted between the glass slide and an 18 × 18 mm #1.5 coverslip in mounting medium (0.5% p-phenylenediamine in 90% glycerol and 20 mM Tris pH 8.8) and stored at −20°C. Acquisitions were carried out using the same microscope as above except without binning and a Nikon APO λS 100×/1.45 oil objective. All immunofluorescence images are maximum projections of Z-stacks with Z-plans acquired every 0.2 µm.

Embryonic viability assays and brood size

Embryonic viability assays were performed at 23°C. For each condition, L4-stage worms were singled onto plates to lay embryos. Each day, for five consecutive days, the worms were transferred to new plates. Embryos were scored after transferring the parent worms and again 24 h later to count the larvae. Embryonic viability was determined as the percentage of live embryos found within the progeny, and brood size was measured as the sum of the larvae.

Image analyses

Image analyses were performed on maximum projections using the Fiji software (Schindelin et al., 2012) and by following the methods described in Hattersley et al. (2018). Briefly, normalized intensities, in Fig. 1 E; Fig. 3 B; Fig. 4, C and D; Fig. 5, E and F; Fig. 7, A and B; Fig. 8; Fig. S1 D; Fig. S2, D and G; Fig. S3 E; Fig. S4; and Fig. S5 A were quantified by drawing a rectangular box around the MII chromosomal set and measuring its area (A_a) and integrated intensity (I_a) at each time point. The background intensity was quantified by measuring the area (A_b) and the integrated intensity of an expanded rectangle (five pixels on every side) (I_b) around the MII chromosomal set. The background signal (B_s) corresponds to the difference in the signal and area between the expanded rectangle and the original one″ $B_s = (I_b - I_a)/((A_b - A_a)/A_a)$. Finally, the normalized integrated intensity over the background corresponds to the difference between the background signal and the intensity of the original signal: $(I_a - B_s)/A_a$. Chromosome segregation in Fig. 3 D and Fig. S5 A was quantified by measuring the distance between the inner surfaces of the chromosome sets over time. The number of oocytes analyzed (*n*) is indicated in the figures and their corresponding legends.

Graphs and statistics

GraphPad Prism 8 (RRID:SCR_002798) was used to generate all graphs and perform statistical tests. In Fig. 3 B; Fig. 4, C and D; Fig. 5 E; Fig. 7 A; Fig. 8; Fig. S2 D; Fig. S3 E; and Fig. S5 A: Mann-Whitney tests on the mean value of GFP::LEM-$2^{LEMD2/3}$ intensity during interkinesis. In Fig. 3 D and Fig. S5 A: Mann–Whitney tests of the mean distance between the segregating chromosomal sets during interkinesis. In Fig. 7 B, Fig. S1 E, and Fig. S4: Mann–Whitney tests of GFP::LEM-$2^{LEMD2/3}$ intensity at the indicated time points. In Fig. 5 F: One-way ANOVA test. *P < 0.05, **P < 0.01, ***P < 0.001, ****P < 0.0001.

Online supplemental material

Five supplementary figures: Fig. S1 shows that the interkinetic envelope is never sealed and that it is negatively regulated by microtubules and the proximity to the plasma membrane. Fig. S2 shows that BAF-1^{BAF} is required for the recruitment of LEM-$2^{LEMD2/3}$ and EMR-1^{Emerin} at the chromosome surface in interkinesis. Fig. S3 shows that MEL-28^{ELYS} is required for the interkinetic envelope integrity. Fig S4 shows the depletion efficiency of various nucleoporins by RNAi. Fig S5 shows that chromosome segregation is not affected by single nucleoporin depletion and that none of the nucleoporin co-depletions resulted in the complete absence LEM-$2^{LEMD2/3}$. 10 supplementary videos: Video 1 is from Fig. 1 B. Video 2 is from Fig. 1 E. Video 3 is from Fig. 2, A and B. Video 4 is from Fig. 2 D. Video 5 is from Fig. 3 A and Fig. 4 F. Video 6 is from Fig. 3 B. Video 7 is from Fig. 5 E. Video 8 is from Fig. 5, C and D. Video 9 is from Fig. 7 A. Video 10 is from Fig. 8. Three supplementary tables: Table S1 shows *C. elegans* strains used in this study. Table S2 shows oligonucleotides used in this study. Table S3 shows antibodies used in this study.

Data availability

All data supporting the findings of this study are available within the paper and its supplementary information.

Acknowledgments

We thank all members of the Dumont lab for their support and advice. We are grateful to Patricia Moussounda, Clarisse Picard, and Téo Bitaille for providing technical support. We thank Anjon Audhya (University of Wisconsin School of Medicine and Public Health, Madison, WI, USA) for the generous gift of antibodies. We acknowledge the ImagoSeine core facility of Institut Jacques

Monod, member of France-BioImaging (ANR-10-INBS-04) and IBiSA, with the support of Labex "Who Am I," Inserm Plan Cancer, Region Ile-de-France and Fondation Bettencourt Schueller.

This work was supported by Centre National de la Recherche Scientifique and University Paris Cité, by National Institutes of Health R01GM117407 and R01GM130764 (J.C. Canman), by a grant from the Spanish Agencia Estatal de Investigación and the European Regional Development Fund PID2019-105069GB-I00 (P. Askjaer), by a fourth-year Ph.D. fellowship from the Ligue Nationale Contre le Cancer RS30J21DOC17_ELMOSSADEQ (L. El Mossadeq), and by a grant from the European Research Council ERC-CoG ChromoSOMe 819179 (J. Dumont).

Author contributions: L. El Mossadeq: Conceptualization, Investigation, Methodology, Visualization, Writing - original draft, Writing - review & editing, L. Bellutti: Investigation, Methodology, R. Le Borgne: Methodology, Visualization, J.C. Canman: Methodology, Writing - review & editing, L. Pintard: Methodology, J.-M. Verbavatz: Methodology, Supervision, P. Askjaer: Methodology, Resources, J. Dumont: Conceptualization, Funding acquisition, Investigation, Methodology, Project administration, Supervision, Visualization, Writing - original draft, Writing - review & editing.

Disclosures: The authors declare no competing interests exist.

Submitted: 20 March 2024
Revised: 24 September 2024
Accepted: 18 November 2024

References

Albertson, D.G., and J.N. Thomson. 1993. Segregation of holocentric chromosomes at meiosis in the nematode, Caenorhabditis elegans. *Chromosome Res.* 1:15–26. https://doi.org/10.1007/BF00710603

Anderson, D.J., and M.W. Hetzer. 2008. Reshaping of the endoplasmic reticulum limits the rate for nuclear envelope formation. *J. Cell Biol.* 182: 911–924. https://doi.org/10.1083/jcb.200805140

Anderson, D.J., J.D. Vargas, J.P. Hsiao, and M.W. Hetzer. 2009. Recruitment of functionally distinct membrane proteins to chromatin mediates nuclear envelope formation in vivo. *J. Cell Biol.* 186:183–191. https://doi.org/10.1083/jcb.200901106

Asencio, C., I.F. Davidson, R. Santarella-Mellwig, T.B. Ly-Hartig, M. Mall, M.R. Wallenfang, I.W. Mattaj, and M. Gorjánácz. 2012. Coordination of kinase and phosphatase activities by Lem4 enables nuclear envelope reassembly during mitosis. *Cell.* 150:122–135. https://doi.org/10.1016/j.cell.2012.04.043

Audhya, A., A. Desai, and K. Oegema. 2007. A role for Rab5 in structuring the endoplasmic reticulum. *J. Cell Biol.* 178:43–56. https://doi.org/10.1083/jcb.200701139

Barger, S.R., L. Penfield, and S. Bahmanyar. 2022. Coupling lipid synthesis with nuclear envelope remodeling. *Trends Biochem. Sci.* 47:52–65. https://doi.org/10.1016/j.tibs.2021.08.009

Barger, S.R., L. Penfield, and S. Bahmanyar. 2023. Nuclear envelope assembly relies on CHMP-7 in the absence of BAF-LEM-mediated hole closure. *J. Cell Sci.* 136:jcs261385. https://doi.org/10.1242/jcs.261385

Bellutti, L., N. Macaisne, L. El Mossadeq, T. Ganeswaran, J.C. Canman, and J. Dumont. 2024. Regulation of outer kinetochore assembly during meiosis I and II by CENP-A and KNL-2/M18BP1 in C. elegans oocytes. *Curr Biol.* 34:4853–4868.e6. https://doi.org/10.1016/j.cub.2024.09.004

Boettcher, B., and Y. Barral. 2013. The cell biology of open and closed mitosis. *Nucleus.* 4:160–165. https://doi.org/10.4161/nucl.24676

Brachner, A., S. Reipert, R. Foisner, and J. Gotzmann. 2005. LEM2 is a novel MAN1-related inner nuclear membrane protein associated with A-type lamins. *J. Cell Sci.* 118:5797–5810. https://doi.org/10.1242/jcs.02701

Cohen, M., N. Feinstein, K.L. Wilson, and Y. Gruenbaum. 2003. Nuclear pore protein gp210 is essential for viability in HeLa cells and Caenorhabditis elegans. *Mol. Biol. Cell.* 14:4230–4237. https://doi.org/10.1091/mbc.e03-04-0260

Cohen-Fix, O., and P. Askjaer. 2017. Cell biology of the Caenorhabditis elegans nucleus. *Genetics.* 205:25–59. https://doi.org/10.1534/genetics.116.197160

De Magistris, P., and W. Antonin. 2018. The dynamic nature of the nuclear envelope. *Curr. Biol.* 28:R487–R497. https://doi.org/10.1016/j.cub.2018.01.073

Deerinck, T.J., E.A. Bushong, A. Thor, and M.H. Ellisman. 2010. NCMIR methods for 3D EM: A new protocol for preparation of biological specimens for serial block face scanning electron microscopy. 6–8.

Deolal, P., J. Scholz, K. Ren, H. Bragulat-Teixidor, and S. Otsuka. 2024. Sculpting nuclear envelope identity from the endoplasmic reticulum during the cell cycle. *Nucleus.* 15:2299632. https://doi.org/10.1080/19491034.2023.2299632

Dey, G., and B. Baum. 2021. Nuclear envelope remodelling during mitosis. *Curr. Opin. Cell Biol.* 70:67–74. https://doi.org/10.1016/j.ceb.2020.12.004

Dumont, J., and A. Desai. 2012. Acentrosomal spindle assembly and chromosome segregation during oocyte meiosis. *Trends Cell Biol.* 22:241–249. https://doi.org/10.1016/j.tcb.2012.02.007

Fernandez, A.G., and F. Piano. 2006. MEL-28 is downstream of the Ran cycle and is required for nuclear-envelope function and chromatin maintenance. *Curr. Biol.* 16:1757–1763. https://doi.org/10.1016/j.cub.2006.07.071

Fernandez-Martinez, J., and M.P. Rout. 2021. One ring to rule them all? Structural and functional diversity in the nuclear pore complex. *Trends Biochem. Sci.* 46:595–607. https://doi.org/10.1016/j.tibs.2021.01.003

Floch, A.G., D. Tareste, P.F. Fuchs, A. Chadrin, I. Naciri, T. Léger, G. Schlenstedt, B. Palancade, and V. Doye. 2015. Nuclear pore targeting of the yeast Pom33 nucleoporin depends on karyopherin and lipid binding. *J. Cell Sci.* 128:305–316. https://doi.org/10.1242/jcs.158915

Fragoso-Luna, A., R. Romero-Bueno, M. Eibl, C. Ayuso, C. Munoz-Jimenez, V. Benes, I. Cases, and P. Askjaer. 2023. Expanded FLP toolbox for spatiotemporal protein degradation and transcriptomic profiling in Caenorhabditis elegans. *Genetics.* 223:iyac166. https://doi.org/10.1093/genetics/iyac166

Franz, C., P. Askjaer, W. Antonin, C.L. Iglesias, U. Haselmann, M. Schelder, A. de Marco, M. Wilm, C. Antony, and I.W. Mattaj. 2005. Nup155 regulates nuclear envelope and nuclear pore complex formation in nematodes and vertebrates. *EMBO J.* 24:3519–3531. https://doi.org/10.1038/sj.emboj.7600825

Franz, C., R. Walczak, S. Yavuz, R. Santarella, M. Gentzel, P. Askjaer, V. Galy, M. Hetzer, I.W. Mattaj, and W. Antonin. 2007. MEL-28/ELYS is required for the recruitment of nucleoporins to chromatin and postmitotic nuclear pore complex assembly. *EMBO Rep.* 8:165–172. https://doi.org/10.1038/sj.embor.7400889

Furuno, N., M. Nishizawa, K. Okazaki, H. Tanaka, J. Iwashita, N. Nakajo, Y. Ogawa, and N. Sagata. 1994. Suppression of DNA replication via Mos function during meiotic divisions in Xenopus oocytes. *EMBO J.* 13: 2399–2410. https://doi.org/10.1002/j.1460-2075.1994.tb06524.x

Galy, V., P. Askjaer, C. Franz, C. López-Iglesias, and I.W. Mattaj. 2006. MEL-28, a novel nuclear-envelope and kinetochore protein essential for zygotic nuclear-envelope assembly in C. elegans. *Curr. Biol.* 16:1748–1756. https://doi.org/10.1016/j.cub.2006.06.067

Gatta, A.T., and J.G. Carlton. 2019. The ESCRT-machinery: Closing holes and expanding roles. *Curr. Opin. Cell Biol.* 59:121–132. https://doi.org/10.1016/j.ceb.2019.04.005

Gerhart, J., M. Wu, and M. Kirschner. 1984. Cell cycle dynamics of an M-phase-specific cytoplasmic factor in Xenopus laevis oocytes and eggs. *J. Cell Biol.* 98:1247–1255. https://doi.org/10.1083/jcb.98.4.1247

Gómez-Saldivar, G., A. Fernandez, Y. Hirano, M. Mauro, A. Lai, C. Ayuso, T. Haraguchi, Y. Hiraoka, F. Piano, and P. Askjaer. 2016. Identification of conserved MEL-28/ELYS domains with essential roles in nuclear assembly and chromosome segregation. *PLoS Genet.* 12:e1006131. https://doi.org/10.1371/journal.pgen.1006131

Gorjánácz, M., E.P.F. Klerkx, V. Galy, R. Santarella, C. López-Iglesias, P. Askjaer, and I.W. Mattaj. 2007. Caenorhabditis elegans BAF-1 and its kinase VRK-1 participate directly in post-mitotic nuclear envelope assembly. *EMBO J.* 26:132–143. https://doi.org/10.1038/sj.emboj.7601470

Greber, U.F., A. Senior, and L. Gerace. 1990. A major glycoprotein of the nuclear pore complex is a membrane-spanning polypeptide with a large lumenal domain and a small cytoplasmic tail. *EMBO J.* 9:1495–1502. https://doi.org/10.1002/j.1460-2075.1990.tb08267.x

Gruenbaum, Y., K.K. Lee, J. Liu, M. Cohen, and K.L. Wilson. 2002. The expression, lamin-dependent localization and RNAi depletion phenotype

for emerin in C. elegans. *J. Cell Sci.* 115:923–929. https://doi.org/10.1242/jcs.115.5.923

Gu, M., D. LaJoie, O.S. Chen, A. von Appen, M.S. Ladinsky, M.J. Redd, L. Nikolova, P.J. Bjorkman, W.I. Sundquist, K.S. Ullman, and A. Frost. 2017. LEM2 recruits CHMP7 for ESCRT-mediated nuclear envelope closure in fission yeast and human cells. *Proc. Natl. Acad. Sci. USA.* 114: E2166–E2175. https://doi.org/10.1073/pnas.1613916114

Hamed, M., and W. Antonin. 2021. Dunking into the lipid bilayer: How direct membrane binding of nucleoporins can contribute to nuclear pore complex structure and assembly. *Cells.* 10:3601. https://doi.org/10.3390/cells10123601

Haraguchi, T., T. Koujin, M. Segura-Totten, K.K. Lee, Y. Matsuoka, Y. Yoneda, K.L. Wilson, and Y. Hiraoka. 2001. BAF is required for emerin assembly into the reforming nuclear envelope. *J. Cell Sci.* 114:4575–4585. https://doi.org/10.1242/jcs.114.24.4575

Harel, A., A.V. Orjalo, T. Vincent, A. Lachish-Zalait, S. Vasu, S. Shah, E. Zimmerman, M. Elbaum, and D.J. Forbes. 2003. Removal of a single pore subcomplex results in vertebrate nuclei devoid of nuclear pores. *Mol. Cell.* 11:853–864. https://doi.org/10.1016/S1097-2765(03)00116-3

Hase, M.E., and V.C. Cordes. 2003. Direct interaction with nup153 mediates binding of Tpr to the periphery of the nuclear pore complex. *Mol. Biol. Cell.* 14:1923–1940. https://doi.org/10.1091/mbc.e02-09-0620

Hattersley, N., D. Cheerambathur, M. Moyle, M. Stefanutti, A. Richardson, K.Y. Lee, J. Dumont, K. Oegema, and A. Desai. 2016. A nucleoporin docks protein phosphatase 1 to direct meiotic chromosome segregation and nuclear assembly. *Dev. Cell.* 38:463–477. https://doi.org/10.1016/j.devcel.2016.08.006

Hattersley, N., P. Lara-Gonzalez, D. Cheerambathur, J.S. Gomez-Cavazos, T. Kim, B. Prevo, R. Khaliullin, K.Y. Lee, M. Ohta, R. Green, et al. 2018. Employing the one-cell C. elegans embryo to study cell division processes. *Methods Cell Biol.* 144:185–231. https://doi.org/10.1016/bs.mcb.2018.03.008

Hetzer, M.W. 2010. The nuclear envelope. *Cold Spring Harb. Perspect. Biol.* 2: a000539. https://doi.org/10.1101/cshperspect.a000539

Huang, G., C. Zeng, and Y. Shi. 2023. Structure of the nuclear pore complex goes atomic. *Curr. Opin. Struct. Biol.* 78:102523. https://doi.org/10.1016/j.sbi.2022.102523

Kremer, J.R., D.N. Mastronarde, and J.R. McIntosh. 1996. Computer visualization of three-dimensional image data using IMOD. *J. Struct. Biol.* 116: 71–76. https://doi.org/10.1006/jsbi.1996.0013

Laband, K., R. Le Borgne, F. Edwards, M. Stefanutti, J.C. Canman, J.M. Verbavatz, and J. Dumont. 2017. Chromosome segregation occurs by microtubule pushing in oocytes. *Nat. Commun.* 8:1499. https://doi.org/10.1038/s41467-017-01539-8

Lachat, J., A. Pascault, D. Thibaut, R. Le Borgne, J.M. Verbavatz, and A. Weiner. 2022. Trans-cellular tunnels induced by the fungal pathogen Candida albicans facilitate invasion through successive epithelial cells without host damage. *Nat. Commun.* 13:3781. https://doi.org/10.1038/s41467-022-31237-z

Lee, K.K., Y. Gruenbaum, P. Spann, J. Liu, and K.L. Wilson. 2000. C. elegans nuclear envelope proteins emerin, MAN1, lamin, and nucleoporins reveal unique timing of nuclear envelope breakdown during mitosis. *Mol. Biol. Cell.* 11:3089–3099. https://doi.org/10.1091/mbc.11.9.3089

Lee, Z.Y., M. Prouteau, M. Gotta, and Y. Barral. 2016. Compartmentalization of the endoplasmic reticulum in the early C. elegans embryos. *J. Cell Biol.* 214:665–676. https://doi.org/10.1083/jcb.201601047

Lénárt, P., and J. Ellenberg. 2003. Nuclear envelope dynamics in oocytes: From germinal vesicle breakdown to mitosis. *Curr. Opin. Cell Biol.* 15: 88–95. https://doi.org/10.1016/S0955-0674(02)00011-X

Lin, D.H., and A. Hoelz. 2019. The structure of the nuclear pore complex (an update). *Annu. Rev. Biochem.* 88:725–783. https://doi.org/10.1146/annurev-biochem-062917-011901

Lin, F., D.L. Blake, I. Callebaut, I.S. Skerjanc, L. Holmer, M.W. McBurney, M. Paulin-Levasseur, and H.J. Worman. 2000. MAN1, an inner nuclear membrane protein that shares the LEM domain with lamina-associated polypeptide 2 and emerin. *J. Biol. Chem.* 275:4840–4847. https://doi.org/10.1074/jbc.275.7.4840

Liu, J., K.K. Lee, M. Segura-Totten, E. Neufeld, K.L. Wilson, and Y. Gruenbaum. 2003. MAN1 and emerin have overlapping function(s) essential for chromosome segregation and cell division in Caenorhabditis elegans. *Proc. Natl. Acad. Sci. USA.* 100:4598–4603. https://doi.org/10.1073/pnas.0730821100

Liu, J., T. Rolef Ben-Shahar, D. Riemer, M. Treinin, P. Spann, K. Weber, A. Fire, and Y. Gruenbaum. 2000. Essential roles for Caenorhabditis elegans lamin gene in nuclear organization, cell cycle progression, and spatial organization of nuclear pore complexes. *Mol. Biol. Cell.* 11: 3937–3947. https://doi.org/10.1091/mbc.11.11.3937

Malone, C.J., L. Misner, N. Le Bot, M.C. Tsai, J.M. Campbell, J. Ahringer, and J.G. White. 2003. The C. elegans hook protein, ZYG-12, mediates the essential attachment between the centrosome and nucleus. *Cell.* 115: 825–836. https://doi.org/10.1016/S0092-8674(03)00985-1

Manilal, S., T.M. Nguyen, C.A. Sewry, and G.E. Morris. 1996. The Emery-Dreifuss muscular dystrophy protein, emerin, is a nuclear membrane protein. *Hum. Mol. Genet.* 5:801–808. https://doi.org/10.1093/hmg/5.6.801

McGillivary, R.M., D.A. Starr, and G.W.G. Luxton. 2023. Building and breaking mechanical bridges between the nucleus and cytoskeleton: Regulation of LINC complex assembly and disassembly. *Curr. Opin. Cell Biol.* 85:102260. https://doi.org/10.1016/j.ceb.2023.102260

Mehsen, H., V. Boudreau, D. Garrido, M. Bourouh, M. Larouche, P.S. Maddox, A. Swan, and V. Archambault. 2018. PP2A-B55 promotes nuclear envelope reformation after mitosis in Drosophila. *J. Cell Biol.* 217: 4106–4123. https://doi.org/10.1083/jcb.201804018

Morales-Martinez, A., A. Dobrzynska, and P. Askjaer. 2015. Inner nuclear membrane protein LEM-2 is required for correct nuclear separation and morphology in C. elegans. *J. Cell Sci.* 128:1090–1096. https://doi.org/10.1242/jcs.164202

Mullen, T.J., A.C. Davis-Roca, and S.M. Wignall. 2019. Spindle assembly and chromosome dynamics during oocyte meiosis. *Curr. Opin. Cell Biol.* 60: 53–59. https://doi.org/10.1016/j.ceb.2019.03.014

Nagano, A., R. Koga, M. Ogawa, Y. Kurano, J. Kawada, R. Okada, Y.K. Hayashi, T. Tsukahara, and K. Arahata. 1996. Emerin deficiency at the nuclear membrane in patients with Emery-Dreifuss muscular dystrophy. *Nat. Genet.* 12:254–259. https://doi.org/10.1038/ng0396-254

Nakajo, N., S. Yoshitome, J. Iwashita, M. Iida, K. Uto, S. Ueno, K. Okamoto, and N. Sagata. 2000. Absence of Wee1 ensures the meiotic cell cycle in Xenopus oocytes. *Genes Dev.* 14:328–338. https://doi.org/10.1101/gad.14.3.328

Nebreda, A.R., and I. Ferby. 2000. Regulation of the meiotic cell cycle in oocytes. *Curr. Opin. Cell Biol.* 12:666–675. https://doi.org/10.1016/S0955-0674(00)00150-2

Nkombo Nkoula, S., G. Velez-Aguilera, B. Ossareh-Nazari, L. Van Hove, C. Ayuso, V. Legros, G. Chevreux, L. Thomas, G. Seydoux, P. Askjaer, et al. 2023. Mechanisms of nuclear pore complex disassembly by the mitotic Polo-like kinase 1 (PLK-1) in C. elegans embryos. *Sci. Adv.* 9. eadf7826. https://doi.org/10.1126/sciadv.adf7826

Ohkura, H. 2015. Meiosis: An overview of key differences from mitosis. *Cold Spring Harb. Perspect. Biol.* 7:a015859. https://doi.org/10.1101/cshperspect.a015859

Otsuka, S., A.M. Steyer, M. Schorb, J.K. Hériché, M.J. Hossain, S. Sethi, M. Kueblbeck, Y. Schwab, M. Beck, and J. Ellenberg. 2018. Postmitotic nuclear pore assembly proceeds by radial dilation of small membrane openings. *Nat. Struct. Mol. Biol.* 25:21–28. https://doi.org/10.1038/s41594-017-0001-9

Penfield, L., R. Shankar, E. Szentgyörgyi, A. Laffitte, M.S. Mauro, A. Audhya, T. Müller-Reichert, and S. Bahmanyar. 2020. Regulated lipid synthesis and LEM2/CHMP7 jointly control nuclear envelope closure. *J. Cell Biol.* 219:e201908179. https://doi.org/10.1083/jcb.201908179

Pitayu-Nugroho, L., M. Aubry, K. Laband, H. Geoffroy, T. Ganeswaran, A. Primadhanty, J.C. Canman, and J. Dumont. 2023. Kinetochore component function in C. elegans oocytes revealed by 4D tracking of holocentric chromosomes. *Nat. Commun.* 14:4032. https://doi.org/10.1038/s41467-023-39702-z

Poteryaev, D., J.M. Squirrell, J.M. Campbell, J.G. White, and A. Spang. 2005. Involvement of the actin cytoskeleton and homotypic membrane fusion in ER dynamics in Caenorhabditis elegans. *Mol. Biol. Cell.* 16:2139–2153. https://doi.org/10.1091/mbc.e04-08-0726

Rasala, B.A., A.V. Orjalo, Z. Shen, S. Briggs, and D.J. Forbes. 2006. ELYS is a dual nucleoporin/kinetochore protein required for nuclear pore assembly and proper cell division. *Proc. Natl. Acad. Sci. USA.* 103: 17801–17806. https://doi.org/10.1073/pnas.0608484103

Ródenas, E., E.P. Klerkx, C. Ayuso, A. Audhya, and P. Askjaer. 2009. Early embryonic requirement for nucleoporin Nup35/NPP-19 in nuclear assembly. *Dev. Biol.* 327:399–409. https://doi.org/10.1016/j.ydbio.2008.12.024

Ródenas, E., C. González-Aguilera, C. Ayuso, and P. Askjaer. 2012. Dissection of the NUP107 nuclear pore subcomplex reveals a novel interaction with spindle assembly checkpoint protein MAD1 in Caenorhabditis elegans. *Mol. Biol. Cell.* 23:930–944. https://doi.org/10.1091/mbc.E11-11-0927

Rolls, M.M., D.H. Hall, M. Victor, E.H. Stelzer, and T.A. Rapoport. 2002. Targeting of rough endoplasmic reticulum membrane proteins and ribosomes in invertebrate neurons. *Mol. Biol. Cell*. 13:1778–1791. https://doi.org/10.1091/mbc.01-10-0514

Samwer, M., M.W.G. Schneider, R. Hoefler, P.S. Schmalhorst, J.G. Jude, J. Zuber, and D.W. Gerlich. 2017. DNA cross-bridging shapes a single nucleus from a set of mitotic chromosomes. *Cell*. 170:956–972.e23. https://doi.org/10.1016/j.cell.2017.07.038

Schellhaus, A.K., P. De Magistris, and W. Antonin. 2016. Nuclear reformation at the end of mitosis. *J. Mol. Biol*. 428:1962–1985. https://doi.org/10.1016/j.jmb.2015.09.016

Schindelin, J., I. Arganda-Carreras, E. Frise, V. Kaynig, M. Longair, T. Pietzsch, S. Preibisch, C. Rueden, S. Saalfeld, B. Schmid, et al. 2012. Fiji: An open-source platform for biological-image analysis. *Nat. Methods*. 9:676–682. https://doi.org/10.1038/nmeth.2019

Severson, A.F., G. von Dassow, and B. Bowerman. 2016. Oocyte meiotic spindle assembly and function. *Curr. Top. Dev. Biol*. 116:65–98. https://doi.org/10.1016/bs.ctdb.2015.11.031

Shumaker, D.K., K.K. Lee, Y.C. Tanhehco, R. Craigie, and K.L. Wilson. 2001. LAP2 binds to BAF.DNA complexes: Requirement for the LEM domain and modulation by variable regions. *EMBO J*. 20:1754–1764. https://doi.org/10.1093/emboj/20.7.1754

Steen, R.L., S.B. Martins, K. Taskén, and P. Collas. 2000. Recruitment of protein phosphatase 1 to the nuclear envelope by A-kinase anchoring protein AKAP149 is a prerequisite for nuclear lamina assembly. *J. Cell Biol*. 150:1251–1262. https://doi.org/10.1083/jcb.150.6.1251

Thomas, L., B. Taleb Ismail, P. Askjaer, and G. Seydoux. 2023. Nucleoporin foci are stress-sensitive condensates dispensable for C. elegans nuclear pore assembly. *EMBO J*. 42. e112987. https://doi.org/10.15252/embj.2022112987

Ungricht, R., and U. Kutay. 2015. Establishment of NE asymmetry—targeting of membrane proteins to the inner nuclear membrane. *Curr. Opin. Cell Biol*. 34:135–141. https://doi.org/10.1016/j.ceb.2015.04.005

Ungricht, R., and U. Kutay. 2017. Mechanisms and functions of nuclear envelope remodelling. *Nat. Rev. Mol. Cell Biol*. 18:229–245. https://doi.org/10.1038/nrm.2016.153

van der Voet, M., C.W.H. Berends, A. Perreault, T. Nguyen-Ngoc, P. Gönczy, M. Vidal, M. Boxem, and S. van den Heuvel. 2009. NuMA-related LIN-5, ASPM-1, calmodulin and dynein promote meiotic spindle rotation independently of cortical LIN-5/GPR/Galpha. *Nat. Cell Biol*. 11:269–277. https://doi.org/10.1038/ncb1834

Vollmer, B., M. Lorenz, D. Moreno-Andrés, M. Bodenhöfer, P. De Magistris, S.A. Astrinidis, A. Schooley, M. Flötenmeyer, S. Leptihn, and W. Antonin. 2015. Nup153 recruits the Nup107-160 complex to the inner nuclear membrane for interphasic nuclear pore complex assembly. *Dev. Cell*. 33:717–728. https://doi.org/10.1016/j.devcel.2015.04.027

Vollmer, B., A. Schooley, R. Sachdev, N. Eisenhardt, A.M. Schneider, C. Sieverding, J. Madlung, U. Gerken, B. Macek, and W. Antonin. 2012. Dimerization and direct membrane interaction of Nup53 contribute to nuclear pore complex assembly. *EMBO J*. 31:4072–4084. https://doi.org/10.1038/emboj.2012.256

Walther, T.C., A. Alves, H. Pickersgill, I. Loïodice, M. Hetzer, V. Galy, B.B. Hülsmann, T. Köcher, M. Wilm, T. Allen, et al. 2003. The conserved Nup107-160 complex is critical for nuclear pore complex assembly. *Cell*. 113:195–206. https://doi.org/10.1016/S0092-8674(03)00235-6

Walther, T.C., M. Fornerod, H. Pickersgill, M. Goldberg, T.D. Allen, and I.W. Mattaj. 2001. The nucleoporin Nup153 is required for nuclear pore basket formation, nuclear pore complex anchoring and import of a subset of nuclear proteins. *EMBO J*. 20:5703–5714. https://doi.org/10.1093/emboj/20.20.5703

Walton, J. 1979. Lead aspartate, an en bloc contrast stain particularly useful for ultrastructural enzymology. *J. Histochem. Cytochem*. 27:1337–1342. https://doi.org/10.1177/27.10.512319

Watson, M.L. 1955. The nuclear envelope; its structure and relation to cytoplasmic membranes. *J. Biophys. Biochem. Cytol*. 1:257–270. https://doi.org/10.1083/jcb.1.3.257

Whaley, W.G., H.H. Mollenhauer, and J.H. Leech. 1960. Some observations on the nuclear envelope. *J. Biophys. Biochem. Cytol*. 8:233–245. https://doi.org/10.1083/jcb.8.1.233

Zhang, L., J.D. Ward, Z. Cheng, and A.F. Dernburg. 2015. The auxin-inducible degradation (AID) system enables versatile conditional protein depletion in C. elegans. *Development*. 142:4374–4384. https://doi.org/10.1242/dev.129635

JCB

Supplemental material

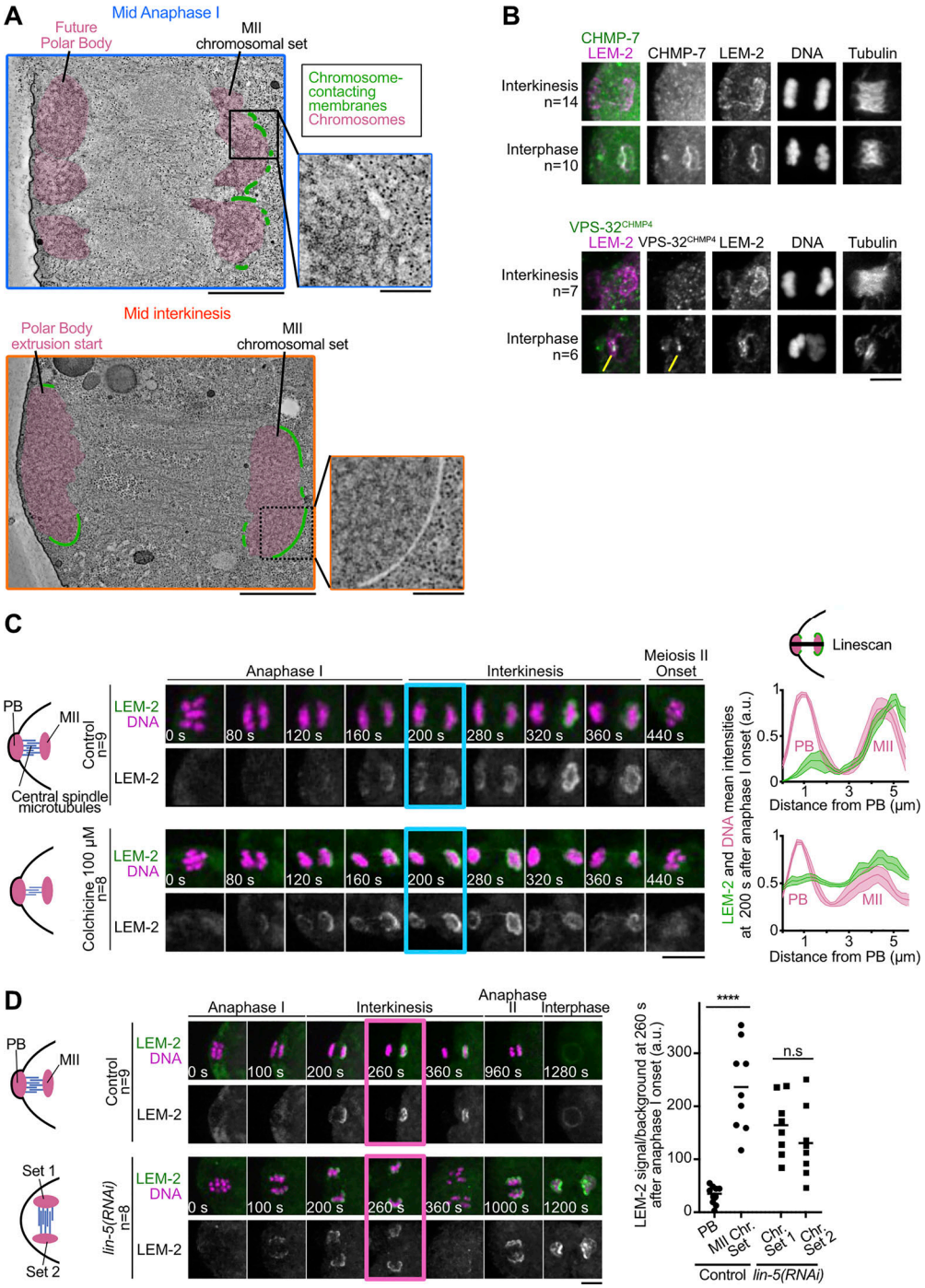

Figure S1. **The interkinetic envelope is never sealed. (A)** Electron tomography sections centered on chromosomes of mid-anaphase I (left) and mid-interkinesis (right) oocytes showing each chromosome set in magenta and membranes in contact with chromosomes in green. Each section is accompanied (right) by a magnification of an ROI centered on a portion of the MII chromosomal set. Scale bar, 1 µm for the full view, 0.25 µm for the magnification. **(B)** Representative images centered on chromosomes of fixed oocytes showing the immunolocalization of LEM-2$^{LEMD2/3}$, DNA, Tubulin, and either CHMP-7^{CHMP7} (top) or VPS-32^{CHMP4} (bottom) in interphase and interkinesis. Yellow arrows indicate the focus of VPS-32^{CHMP4} at the site of envelope sealing in interphase. Scale bar, 5 µm. **(C)** Left: Schematics of chromosomes and anaphase I central spindle microtubules in the indicated conditions. Middle: Representative time-lapse images centered on chromosomes of oocytes expressing mCherry::H2B (magenta) and GFP::LEM-2$^{LEMD2/3}$ (green) during meiosis I and II in the indicated conditions. Timings indicated at the bottom left corners of images are from anaphase I onset. The specific meiotic stage used for the quantification is highlighted in cyan. Scale bar, 5 µm. Right: Quantifications of LEM-2$^{LEMD2/3}$ and DNA mean intensities at 200 s after anaphase I onset in the indicated conditions. **(D)** Left: Schematics of chromosomes and spindle orientation in indicated conditions. Middle: Representative time-lapse images centered on chromosomes of oocytes expressing mCherry::H2B (magenta) and GFP::LEM-2$^{LEMD2/3}$ (green) during meiosis I and II in the indicated conditions. Timings indicated at the bottom left corners of images are from anaphase I onset. The timing used for the quantification is highlighted in pink. Scale bar, 5 µm. Right: Quantification of the normalized GFP::LEM-2$^{LEMD2/3}$ integrated intensity at 260 s after anaphase I onset. Error bars correspond to the standard deviation. Mann–Whitney test (****$P < 0.0001$).

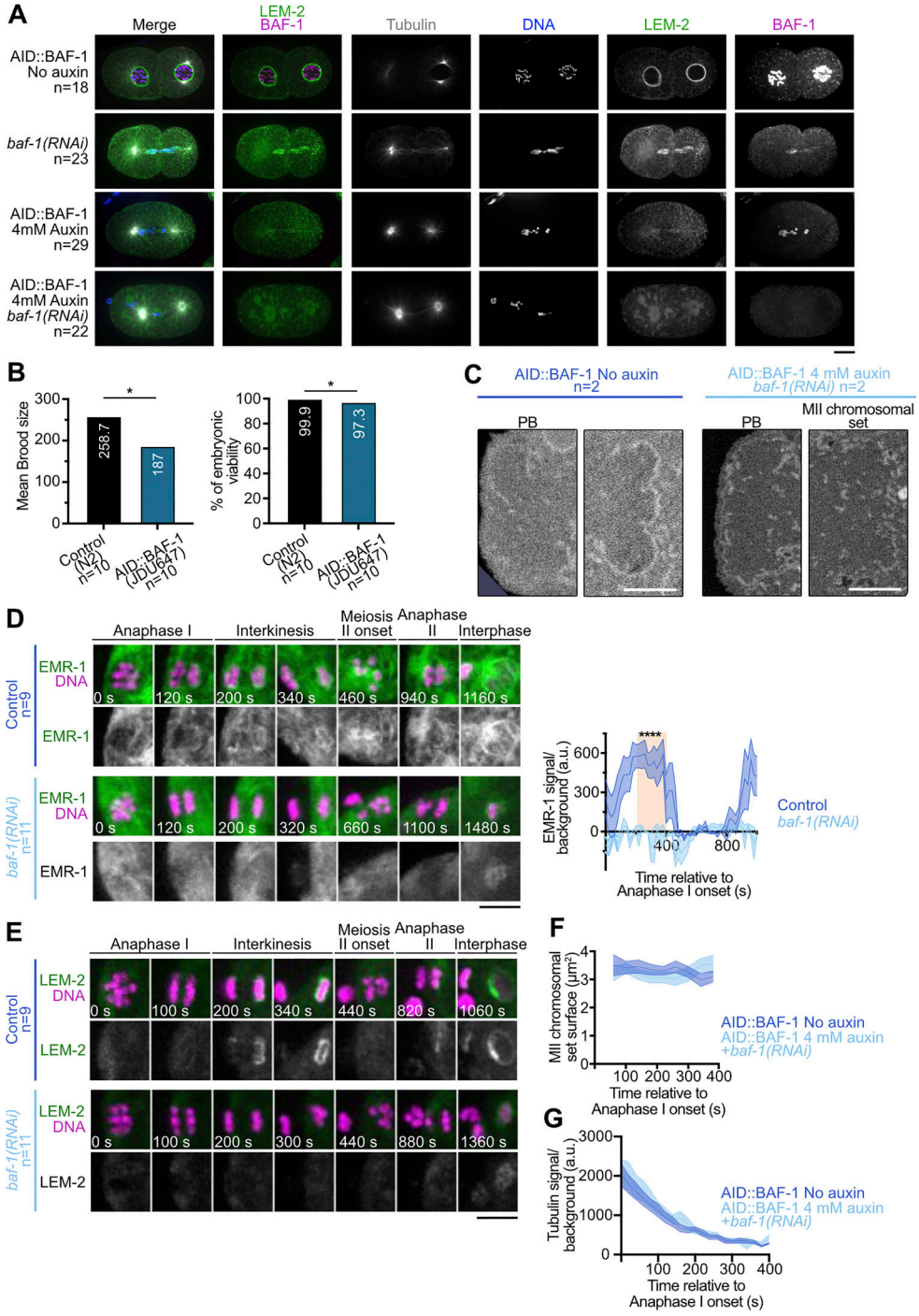

Figure S2. **BAF-1^{BAF} is required for the recruitment of LEM-2$^{LEMD2/3}$ and EMR-1^{Emerin} at the chromosome surface in interkinesis. (A)** Representative images centered on chromosomes of fixed embryos showing the immunolocalization of LEM-2$^{LEMD2/3}$, DNA, Tubulin, and BAF-1^{BAF} during pronuclei migration in control conditions, *baf-1(RNAi)*, and/or 4 mM auxin treatment. Scale bar, 5 µm. **(B)** Quantifications of the mean brood size (left) and the percentage of embryonic viability (right) in N2 (control) and JDU647 (AID::BAF-1^{BAF}) strains. *P < 0.05. **(C)** Two-dimensional single sections of two ROIs centered on each chromosomal set of a control oocyte (AID::BAF-1^{BAF}, No auxin) (top) and a BAF-1^{BAF}–depleted oocyte (AID::BAF-1^{BAF}, 4 mM auxin, *baf-1(RNAi)*). Scale bar, 1 µm. **(D)** Left: Representative time-lapse images centered on chromosomes of oocytes expressing mCherry::H2B (magenta) and GFP::EMR-1^{Emerin} (green) during meiosis I and II in the indicated conditions. Timings indicated at the bottom left corners of images are from anaphase I onset. Scale bar, 5 µm. Right: Quantification of the GFP::EMR-1^{Emerin} integrated intensity normalized over a background from anaphase I onset to interphase for the MII chromosomal set. Control in dark blue, *baf-1(RNAi)* in light blue. Error bars correspond to the standard error of the mean. The orange box indicates interkinesis. Mann–Whitney test on the mean value of GFP::EMR-1^{Emerin} intensity in interkinesis (****P < 0.0001). **(E)** Representative time-lapse images centered on chromosomes of oocytes expressing mCherry::H2B (magenta) and GFP::LEM-2$^{LEMD2/3}$ (green) during meiosis I and II in the indicated conditions. Timings indicated at the bottom left corners of images are from anaphase I onset. Scale bar, 5 µm. The same control oocyte is displayed in Fig. 1 E and Fig. S3 D. **(F and G)** Quantifications of the surface of the MII chromosomal set (F) and of tubulin intensity (G) over time from anaphase I onset in control oocytes (dark blue) and BAF-1^{BAF}–depleted oocytes (light blue). Error bars correspond to the standard error of the mean.

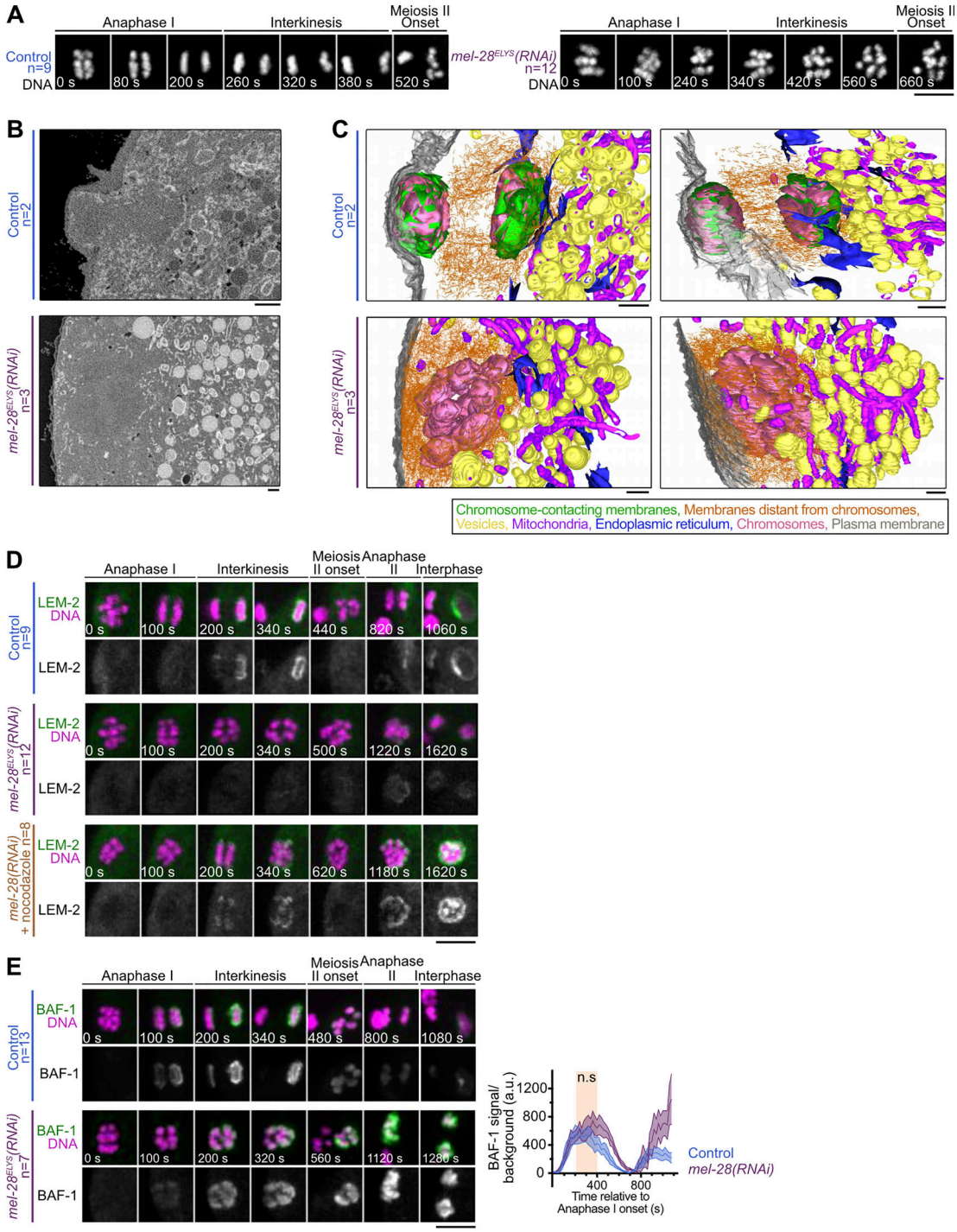

Figure S3. **MEL-28^{ELYS} is required for the interkinetic envelope integrity. (A)** Representative time-lapse images centered on chromosomes of oocytes expressing mCherry::H2B (gray) during anaphase I and interkinesis in the indicated conditions. Timings indicated at the bottom left corners of images are from anaphase I onset. Scale bar, 5 µm. **(B)** Two-dimensional single sections of two ROIs centered on each chromosomal set of a control (top) and a MEL-28^{ELYS}–depleted (bottom) oocyte. Scale bars, 1 µm. **(C)** Three-dimensional reconstructions centered on chromosomes of a control oocyte (top) and a MEL-28^{ELYS}-depleted oocyte (bottom) viewed from two different angles. Scale bar, 1 µm. Chromosomes in magenta, membranes in contact with chromosomes in green, membranes distant from chromosomes in orange, vesicles in yellow, mitochondria in purple, endoplasmic reticulum in blue, and plasma membrane in gray. Scale bars, 1 µm. **(D)** Representative time-lapse images centered on chromosomes of oocytes expressing mCherry::H2B (magenta) and GFP::LEM-2$^{LEMD2/3}$ (green) during meiosis I and II in the indicated conditions. Timings indicated at the bottom left corners of images are from anaphase I onset. Scale bar, 5 µm. The same control oocyte is displayed in Fig. 1 E and Fig. S2 E. **(E)** Left: Representative time-lapse images centered on chromosomes of oocytes expressing mCherry::H2B (magenta) and GFP::BAF-1^{BAF} (green) during meiosis I and II in the indicated conditions. Timings indicated at the bottom left corners of images are from anaphase I onset. Scale bar, 5 µm. Right: Quantification of the GFP::BAF-1^{BAF} integrated intensity normalized over background from anaphase I onset to interphase for the MII chromosomal set. Control in dark blue, *mel-28(RNAi)* in purple. Error bars correspond to the standard error of the mean. The orange box indicates interkinesis. Mann-Whitney test on the mean value of GFP::BAF-1^{BAF} intensity in interkinesis.

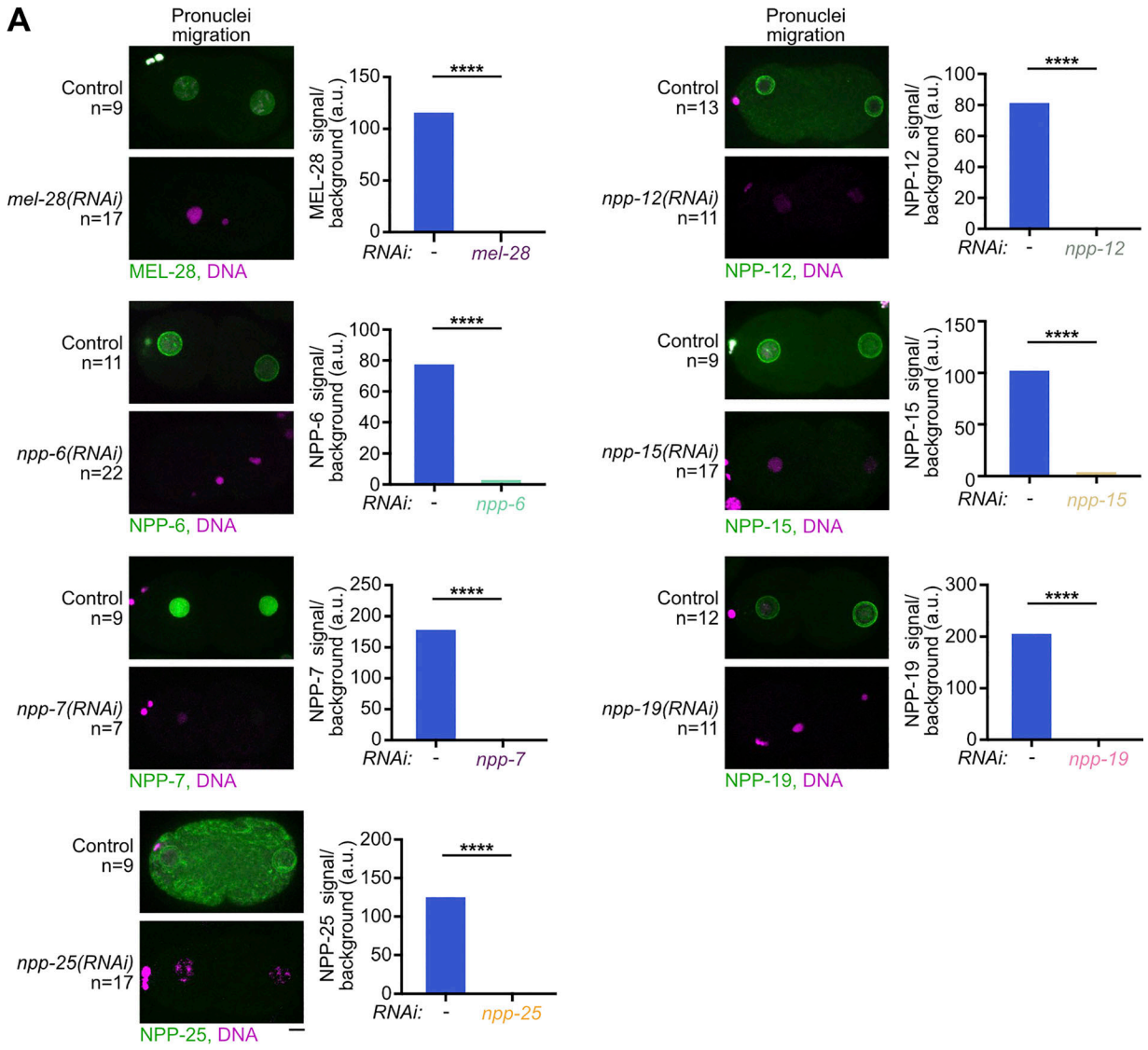

Figure S4. **Depletion efficiency of various nucleoporins by RNAi. (A)** Left: Representative images centered on chromosomes of embryos expressing mCherry::H2B (magenta) and either GFP-tagged MEL-28^{ELYS}, NPP-6^{NUP160}, NPP-15^{NUP133}, NPP-25^{TMEM33}, NPP-12^{NUP210}, NPP-19^{NUP35}, or NPP-7^{NUP153} (green) during pronuclei migration in the indicated conditions. Scale bar, 5 µm. Right: Quantification of the normalized GFP-tagged MEL-28^{ELYS}, NPP-6^{NUP160}, NPP-15^{NUP133}, NPP-25^{TMEM33}, NPP-12^{NUP210}, NPP-19^{NUP35}, or NPP-7^{NUP153} integrated intensity in an ROI centered around the maternal and paternal pronuclei in the indicated conditions. Error bars correspond to the standard error of the mean. Mann–Whitney test (****P < 0.0001).

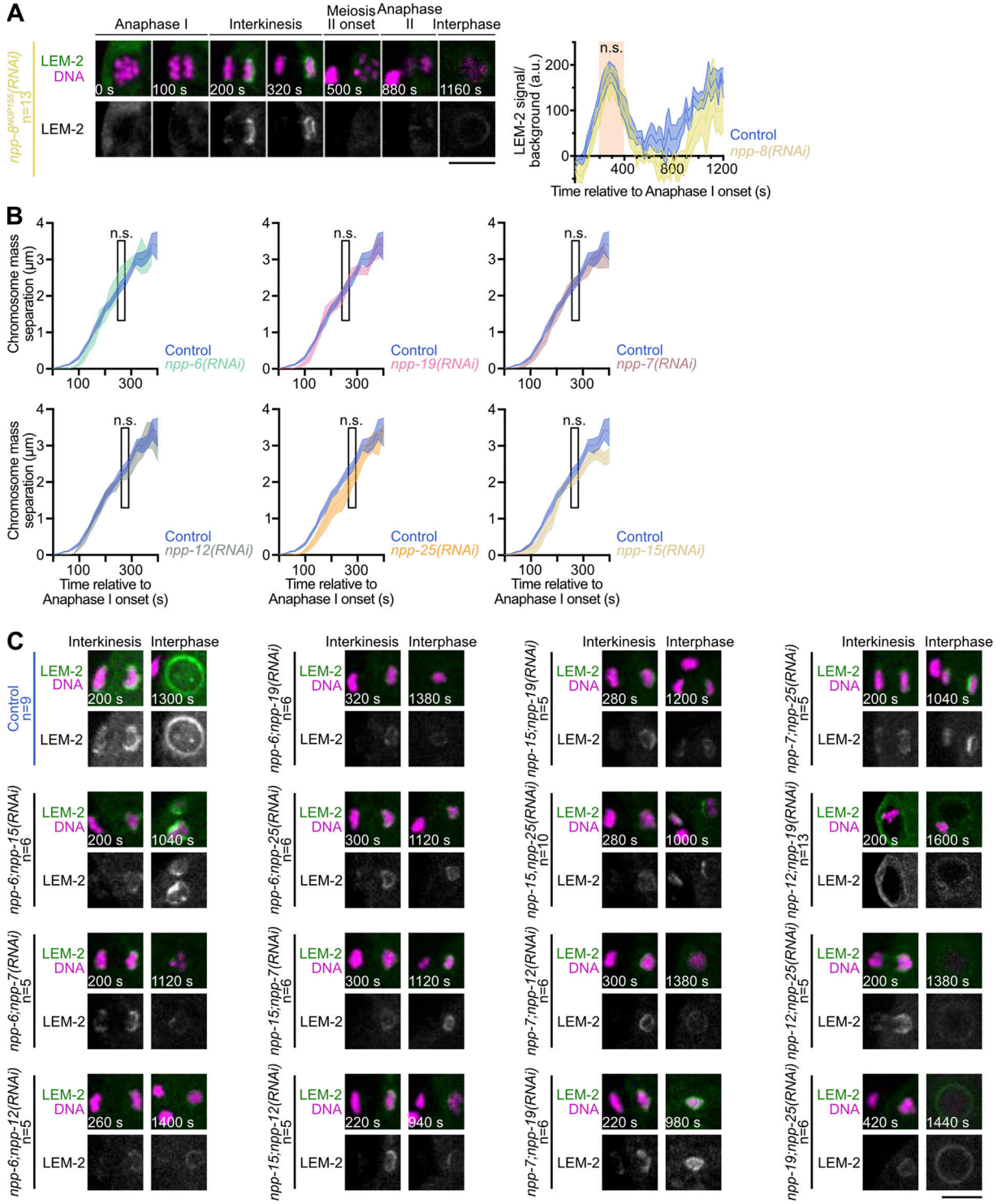

Figure S5. **Nucleoporins with potential membrane-binding domains could contribute to interkinetic envelope integrity but not to chromosome segregation. (A)** Left: Representative time-lapse images centered on chromosomes of oocytes expressing mCherry::H2B (magenta) and GFP::LEM-2$^{LEMD2/3}$ (green) during meiosis I and II in the indicated conditions. Timings indicated at the bottom left corners of images are from anaphase I onset. Scale bar, 5 µm. Right: Quantification of the GFP::LEM-2$^{LEMD2/3}$ integrated intensity normalized over a background from anaphase I onset to interphase for the MII chromosomal set. Control in dark blue, *npp-8(RNAi)* in yellow. Error bars correspond to the standard error of the mean. The orange box indicates interkinesis. Mann–Whitney test on the mean value of GFP::LEM-2$^{LEMD2/3}$ intensity in interkinesis. **(B)** Quantification of the distance between the two sets of segregating chromosomes over time from anaphase I onset. Control in dark blue, *npp-6^{NUP160}(RNAi)* in turquoise, *npp-25^{TMEM33}(RNAi)* in dark orange, *npp-15^{NUP133}(RNAi)* in light orange, *npp-12^{NUP210}(RNAi)* in gray, *npp-19^{NUP53}(RNAi)* in pink and *npp-7^{NUP153}(RNAi)* in light brown. Mann–Whitney test on the mean distance between the segregating chromosomal sets during interkinesis in both conditions. **(C)** Representative time-lapse images centered on chromosomes of oocytes expressing mCherry::H2B (magenta) and GFP::LEM-2$^{LEMD2/3}$ (green) during interkinesis and interphase in the indicated conditions. Timings indicated at the bottom left corners of images are from anaphase I onset. Scale bar, 5 µm.

Video 1. **The video is related to** Fig. 1 B**: Ultrastructure of the interkinetic envelope throughout anaphase I and interkinesis.** Three-dimensional reconstructions centered on chromosomes of mid-anaphase I (left), mid-interkinesis (center), and late interkinesis (right) oocytes. Chromosomes in magenta, membranes in contact with chromosomes in green, and plasma membrane in gray. Scale bar, 1 µm. Playback speed, 7 frames/second.

Video 2. **The video is related to** Fig. 1 E**: LEM-2$^{LEMD2/3}$ localization in meiosis I and II.** Time-lapse imaging of an oocyte expressing mCherry::H2B (magenta) and GFP::LEM-2$^{LEMD2/3}$ (green) during the meiotic and first mitotic division. Timings indicated are from anaphase I onset and images were acquired every 20 s. Scale bar, 5 µm. Playback speed, 7 frames/second.

Video 3. **The video is related to** Fig. 2, A and B**: The interkinetic envelope contains inner, but lacks outer, nuclear membrane proteins.** Time-lapse imaging of oocytes expressing mCherry::H2B (magenta) and either GFP::EMR-1^{Emerin}, GFP::BAF-1^{BAF}, GFP::LMN-1$^{Lamin\ A}$, SUN-1^{SUN1}::GFP, GFP::ZYG-12, GFP::SPCS-1^{SP12}, or GFP::SERP-1.1^{RAMP4} during meiosis I and II. Timings indicated are from anaphase I onset and images were acquired every 20 s. Scale bar, 5 µm. Playback speed, 7 frames/second.

Video 4. **The video is related to** Fig. 2 D**: The interkinetic envelope is not connected to the endoplasmic reticulum.** Three-dimensional reconstructions centered on chromosomes of mid-anaphase I (left) and late interkinesis (right) oocytes. Chromosomes in magenta, membranes in contact with chromosomes in green, plasma membrane in gray, eggshell in gold, and endoplasmic reticulum in blue. Scale bar, 1 µm. Playback speed, 7 frames/second.

Video 5. **The video is related to** Fig. 3 A **and** Fig. 4 F**: BAF-1^{BAF} and VRK-1^{vrk1} are essential for interkinetic envelope integrity.** Three-dimensional reconstructions centered on chromosomes of control (AID::BAF-1^{BAF}, No auxin, No RNAi) (top), BAF-1^{BAF}–depleted (AID::BAF-1^{BAF}, 4 mM auxin, *baf-1(RNAi)*) (middle), and VRK-1^{vrk1}–depleted (*vrk-1(RNAi)*) (bottom) oocytes. Chromosomes in magenta, membranes in contact with chromosomes in green, and plasma membrane in gray. Scale bar, 1 µm. Playback speed, 7 frames/second.

Video 6. **The video is related to** Fig. 3 B**: BAF-1^{BAF} is essential for LEM-2$^{LEMD2/3}$ localization in interkinesis.** Time-lapse imaging of oocytes expressing mCherry::H2B (magenta) and GFP::LEM-2$^{LEMD2/3}$ (green) during meiosis I and II in the indicated conditions. Timings indicated are from anaphase I onset and images were acquired every 20 s. Scale bar, 5 µm. Playback speed, 7 frames/second.

Video 7. **The video is related to** Fig. 5 E**: MEL-28^{ELYS} is essential for LEM-2$^{LEMD2/3}$ localization in interkinesis.** Time-lapse imaging of oocytes expressing mCherry::H2B (magenta) and GFP::LEM-2$^{LEMD2/3}$ (green) during meiosis I and II in the indicated conditions. Timings indicated are from anaphase I onset and images were acquired every 20 s. Scale bar, 5 µm. Playback speed, 7 frames/second.

Video 8. **The video is related to** Fig. 5, C and D**: MEL-28^{ELYS} is required for interkinetic envelope integrity.** 3-dimensional reconstructions centered on chromosomes of a control (top) and a MEL-28^{ELYS}-depleted (bottom) oocytes. Chromosomes in magenta, membranes in contact with chromosomes in green, membranes distant from chromosomes in orange, vesicles in yellow, mitochondria in purple, endoplasmic reticulum in blue, and plasma membrane in gray. Scale bar, 1 µm. Playback speed, 7 frames/second.

Video 9. **The video is related to** Fig. 7 A**: Nucleoporins with a membrane-binding domain could contribute to interkinetic envelope integrity.** Time-lapse imaging of oocytes expressing mCherry::H2B (magenta) and GFP::LEM-2$^{LEMD2/3}$ (green) during meiosis I and II in the indicated conditions. Timings indicated are from anaphase I onset and images were acquired every 20 s. Scale bar, 5 µm. Playback speed, 7 frames/second.

Video 10. **The video is related to** Fig. 8**: The localization of nucleoporins with membrane-binding domains is partially or entirely dependent on MEL-28^{ELYS}.** Time-lapse imaging of oocytes expressing mCherry::H2B (magenta) and either GFP-tagged NPP-6^{NUP160}, NPP-15^{NUP133}, NPP-25^{TMEM33}, or NPP-7^{NUP153} (green) during meiosis I and II in the indicated conditions. Timings indicated are from anaphase I onset and images were acquired every 20 s. Scale bar, 5 µm. Playback speed, 7 frames/second.

Provided online are Table S1, Table S2, and Table S3. Table S1 shows *C. elegans* strains used in this study. Table S2 shows oligonucleotides used in this study. Table S3 shows antibodies used in this study.